Assessment of Cerebrovascular Reactivity in Patients with Brain Metastases

C.J. Guichelaar

Augustus, 19 2021
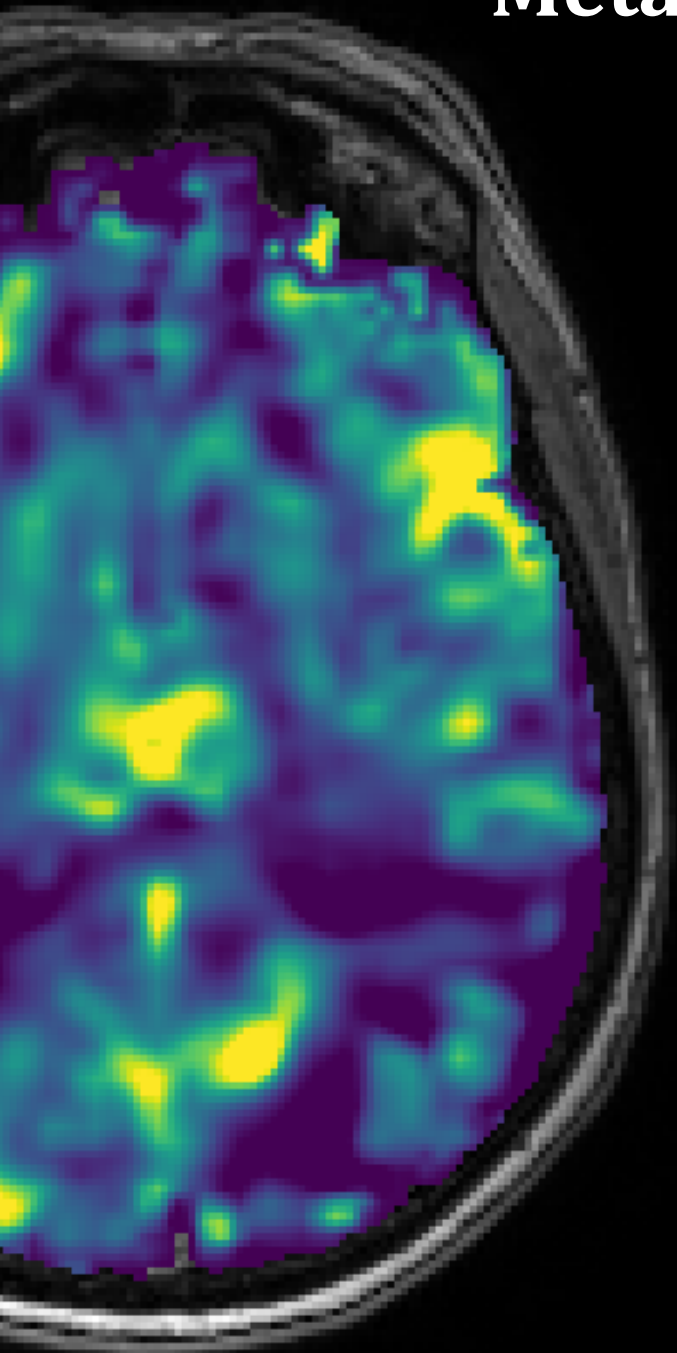
UMC Utrecht

TUDelft

Assessment of Cerebrovascular Reactivity in Patients with Brain Metastases

by

C.J. Guichelaar

to obtain the degree of Master of Science
at the Delft University of Technology,
to be defended publicly on Thursday August 19, 2021 at 13:30.

An electronic version of this thesis is available at `http://repository.tudelft.nl/`.

T̃UDelft   **UMC Utrecht**

Abbreviations

γ	Gyromagnetic Ratio
B	Magnetic Field
B_0	Main Magnetic Field of the MRI
M_0	Net Magnetisation in Longitudinal Direction
v_0	Frequency of the Spins
APRICOT	Assessing and Predicting Radiation Influence on Cognitive Outcome using the cerebrovascular stress Test
AP	Anterior Posterior
BBR	Boundary-Based Registration
BET	Brain Extraction Tool
BM	Brain Metastases
BOLD	Blood Oxygenation Level-Dependent
CBF	Cerebral Blood Flow
CMRO$_2$	Cerebral Metabolic Rate of Oxygen
CO$_2$	Carbon dioxide
corratio	Correlation Ratio
CO	Oxygen Content
CT	Computed Tomography
CVR	Cerebrovascular reactivity
DOF	Degrees of Freedom
EPI	Echo Planar Imaging
EQD$_2$	Equivalend Dose per 2 Gy Fractions
FLAIR	Fluid attenuated inversion recovery
HRF	Hemodynamic Response Function
leastsq	Least Squares
METC	Medical Ethics Review Committee (in Dutch: Medisch Ethische Toetsings Commissie)
MRI	magnetic resonance imaging

mutualinfo	Mutual Information
NN	Nearest Neighbour
normcor	Normalised Correlation
normmi	Normalised Mutual Information
OEF	Oxygen Extraction Fraction
PA	Posterior Anterior
PCO$_2$	Partial Pressure of Carbon Dioxide
PO$_2$	Partial Pressure of Dioxide
RF-pulse	Radiofrequency pulse
RT	Radiotherapy
SRS	Stereotactic radiosurgery
TE	Echo Time
TFE	Turbo Field Echo
TIR	Turbo Inversion Recovery
TI	Inversion Time
TR	Repetition Time
UMC	University Medical Center
WBRT	Whole-brain Radiotherapy
WMO Act	Medical Research Involving Human Subjects Act

Acknowledgements

Contents

Abstract

Introduction: Radiation is an effective treatment to increase the overall mean survival of patients with metastatic brain tumours, however, damage to healthy tissue is inevitable. Radiation can cause dysfunction of the cerebrovasculature, which is hypothesised to induce cognitive decline in patients after radiotherapy (RT). A new method, the cerebrovascular stress test, is able to visualise cerebrovascular reactivity (CVR), which is the ability of the vessels to dilate after a vasoactive stimulus. Research suggests a link between reduced CVR and cognitive impairment in patients, however, current studies have not yet shown if CVR is reduced in patients with metastatic brain tumours. This thesis aims to assess CVR in patients with metastatic brain tumours at baseline and after RT.

Methods: In this thesis, 13 patients with metastatic brain metastases were included and underwent a magnetic resonance imaging (MRI) scan with a vasoactive stimulus at baseline and three months after the same MRI scan with stimulus. On the same day as the baseline MRI scan, the patients received RT. CVR maps were calculated using the MRI scan with the vasoactive stimulus. An additional computed tomography scan was obtained from each patient prior to their first MRI scan. All scanning data was brought into spatial correspondence with a developed image registration pipeline. After the scanning data was registered image analysis was performed using a VOI- and dose-based analysis.

Results: The performance of the image registration pipeline was close to optimal for the MRI scans, and 69% for the baseline CT scan. The image analysis found a significant increase of CVR at an increasing distance from the tumour for white matter (WM) (p = 0.050). For grey matter (GM) and WM, a significant increase of CVR was found at 14 pixels away from the tumour in comparison to 2 pixels away from the tumour (WM: p = 0.039, and GM: p = 0.046). In the dose-based analysis, a nonsignificant decrease of mean CVR was found after RT. The decrease in CVR after RT did also not depend on the received dose.

Conclusions: This thesis developed an image registration pipeline that can be used in further analysis with this specific patient group and scanning data. The image analysis showed a significant increase in CVR at a distance from the tumour for GM and WM. These results indicate that BM influences the CVR of these patients. However, no conclusions can be drawn based on the dose-based analysis. Additional research needs to be done to relate changes in CVR to cognitive decline in patients with metastatic brain tumours.

Keywords: Cerebrovascular Reactivity, Image Registration Pipeline, Image Analysis, Radiotherapy, MRI, CT

1

1 Introduction

Brain metastases (BM) occur in 20% to 40% of patients with cancer [1, 2] and are most commonly caused by melanoma, lung cancer, and breast cancer [3]. The most common treatment options are radiotherapy (RT), an operation, chemotherapy, or a combination of these treatments [4]. The choice of treatment depends on various aspects, such as the characteristics of the tumour, medical history of the patient, and the general state of health of the patient [2, 5].

The mainstay treatment is RT, and the treatment options for RT can be divided into whole-brain RT (WBRT) and stereotactic radiosurgery (SRS) [6, 7]. WBRT irradiates the entire brain to sterilise potential not yet visible BMs [8]. SRS delivers the treatment dose locally in a single fraction and reduces the exposure of healthy brain tissue [7]. Although both treatment options have an equal overall mean survival, cognitive decline is more common in patients that received WBRT. [9–11]. Cognitive decline can have a devastating impact on patients' quality of life [12–14] because it can manifest itself as memory loss, loss of attention span or other cognitive ability loss [15, 16]. These patients have an average mean survival of only seven months if they receive treatment [17]. Therefore, maintaining a good quality of life in these last months is important and should influence the treatment of these patients.

Radiation-induced cognitive decline occurs in up to 50-90% of the brain tumour patients that survived six months after their irradiation treatment [18]. The cause of radiation-induced cognitive decline is not yet fully understood. However, evidence suggests that one of the factors that could cause radiation-induced cognitive decline is vascular insufficiency. This insufficiency is caused by early forms of radiation-induced damage that can lead to ischemia and induce neuronal death [19].

Irradiation treatment causes cerebrovascular injury that can alter the vasculature and its function [18]. These alterations can include blood vessel dilation, endothelial cell damage, and capillary loss, which can lead to disruption of the blood-brain barrier, increased blood-brain barrier permeability and oedema in the brain [18, 20–22]. Additionally, RT can cause cerebral microvascular rarefaction in structures that are important for cognitive functions [23]. Microvascular rarefaction is the loss of or decrease in capillary density [24] and might also be associated with the development of cognitive impairment in patients after RT [25]. The function of cerebrovasculature can be measured with a new technique: the cerebrovascular stress test [26, 27]. This technique measures the ability of the vasculature to regulate blood flow after a vasodilatory stimulus, which is also referred to as the cerebrovascular reactivity (CVR) [28].

The measurements of this test can be visualised in a CVR map that can be acquired with an advanced magnetic resonance imaging (MRI) technique while delivering an external vasoactive stimulus. This stimulus aims to increase carbon dioxide (CO_2) concentration in blood to stimulate the cerebrovasculature to dilate. CVR maps may explain the connection between cognitive function and brain vascular function because diminished vascular function may depict itself as a reduced CVR in a CVR map [27]. Evidence suggests a link between a reduced CVR and mild cognitive impairment [29]. Another study also showed that reduced CVR is related to lower cognitive testing scores in participants [30].

Research suggests a link between reduced CVR and cognitive decline. However, it is not yet established if BM influences the CVR in surrounding vasculature in patients with BM and if CVR is reduced after RT in patients with BM. This research aims to assess this by evaluating

the CVR of patients with BM at baseline and after RT. This is accomplished by obtaining CVR maps of patients with MRI while they are undergoing an external breathing stimulus before (baseline) and three months after RT (follow-up). The obtained data is analysed in a developed image analysis pipeline that registers the data, removes certain artefacts, and analyses the CVR data.

This report will give background information on basic brain anatomy, the workings of an MRI scanner, the MRI sequences used in this study, CVR, and image registration. Afterwards, the development of the image analysis pipeline and the process of the CVR analysis is discussed. Subsequently, results of the image registration pipeline and the CVR analysis will be presented and limitations will be discussed. Finally, the report will elaborate on prospects for future research on this subject.

2 Preliminaries

This chapter will provide background information on basic brain anatomy, the workings of MRI, the three MRI sequences that were used in this thesis, and the mechanics behind the cerebral vascular stress test. In the last section of this chapter, information about image registration will be explained.

2.1 Brain anatomy

The brain can be divided into two matters, white (WM) and grey matter (GM). Surrounding the brain is a clear fluid that is called cerebral spinal fluid (CSF). This fluid is also located inside the ventricles of the brain [31]. Figure 1 shows an example of an MRI scan of the brain. GM is composed of neuron cell bodies, non-neuronal cells that support the neurons, and blood vessels. WM mainly consist of fibre bundles and is responsible for communication between cerebral areas [31]. The density of capillaries is much lower in WM than in GM [32]. Therefore, most of the expected response during the cerebral vascular stress test is from GM.
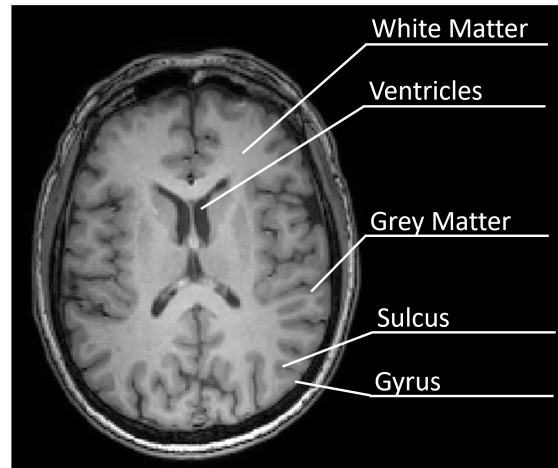
Fig. 1. MRI scan of the brain where different anatomical structures are specified.

2.2 Magnetic Resonance Imaging

Certain atomic nuclei become magnetised when placed in an external magnetic field. In MRI, the focus is typically on hydrogen nuclei. These hydrogen nuclei have spin, which is a fundamental property of nature. The protons in the nuclei will behave like tiny rotating magnets and have two different rotations, one around its axis and one around the second axis. The latter rotation is also referred to as precession. The sum of all these tiny magnets is net magnetisation. When the tiny magnets are placed inside a large external magnetic field (B_0), the spins will align with this field. In Figure 2, the precession of a dipole in the direction of B_0 of a magnetic dipole is illustrated [33].

When a patient is placed inside the MRI scanner, protons inside the body will align with B_0. This alignment in the direction of B_0 means that the net magnetisation (M_0) is in the longitudinal direction. To create an image, the longitudinal net magnetisation needs to be flipped into the transverse plane. This can be accomplished by producing a radiofrequency (RF) pulse that tips the net magnetisation partially (¡90°) or completely (90°) into the transverse plane. After the RF-pulse, the net magnetisation is flipped into the transverse plane, and the protons start to precess in phase (see Figure 3a and 3b). The net magnetisation in the transverse plane creates a signal that can be picked up by the MRI scanner [34]. The precession

frequency of the spins (v_0) is proportional to the magnetic field it is experiencing (B) and the gyromagnetic ratio (γ), which is different for each nucleus (Equation 1). [34]

$$v_o = B\gamma \tag{1}$$

After the net magnetisation is flipped into the transverse plane, the RF-pulse (also referred to as the excitation pulse) is switched off. The protons start to dephase, and the net magnetisation will return to the longitudinal direction. This process is called T1 relaxation. The disappearance of the magnetisation in the transverse plane is referred to as T2 relaxation. The differences between T1 and T2 relaxation times for each type of tissue allows for physiological contrast in MRI images. Water has a long T1 and T2 time, and fat has a short T1 and T2 time.

Part of the T2 relaxation is due to the recovery of the longitudinal magnetisation, but most of the relaxation is caused by dephasing of the spins in the transverse plane. Dephasing is caused by molecular interaction between the spins (pure T2-relaxation) and field inhomogeneities in the magnetic field (T2*-relaxation). The dephasing caused by molecular interaction is random and cannot

Fig. 2. Illustration of a magnetic dipole that is precessing in the direction of the main magnetic field. The ring visualises the precessing motion of the magnetic dipole. This image is reproduced and adapted from a book written by Buxton et al. [34]

be influenced. The field inhomogeneities are constant and will not change as long as the patient is inside the scanner. [34, 36]

The process of relaxation is quick, and the signal of the spins in the transverse plane decay exponentially. Fast exponential decay of the signal does not provide sufficient time for the MRI scanner to sample all data within one repetition time (TR). A TR is a time between each RF-pulse. This issue can be combatted with the generation of echoes. An echo is created by returning the signal after it has been decayed by reversing the dephasing of the spins. The time between the RF-pulse and the echo is called the echo time (TE).

There are two main types of methods to generate these echoes, the spin echo and the gradient echo technique. Spin echo techniques involve the application of a 180° pulse after the 90° RF-pulse to refocus the dephasing of the spins. This results in an echo that has a slightly weaker signal than the signal after the 90° RF-pulse. Conversely, the gradient echo uses a single RF-pulse followed by the application of a gradient to generate the echo. The spin and gradient echo are visualised in Figure 4 [37]. In this study, both techniques are used. The T1-weighted (T1) scan and the BOLD scan uses the gradient technique, and the T2-weighted FLAIR (Fluid attenuated inversion recovery) scan makes use of the spin echo technique.

Additionally, other gradients are used to provide spatial information. These gradients vary linearly in strength, and the strength depends on the position and the area that is being scanned. The spatial information is obtained with three separately positioned gradients in the x-, y- and z-direction. A slice selection gradient is used to select an anatomical volume of interest. This gradient, for example, creates a lower magnetic field in the neck of the patient that linearly
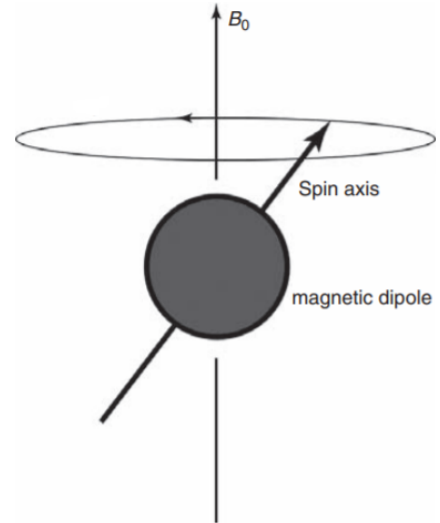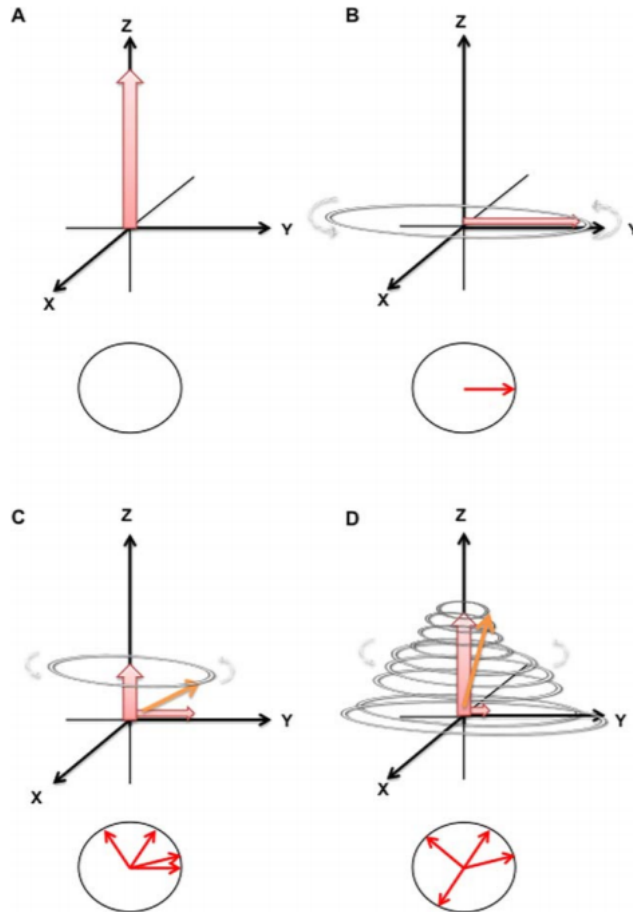
Fig. 3. Recovery of longitudinal magnetisation after an RF-pulse of 90°. A) The protons are aligned with B_0 in the z-direction. B) The net magnetisation is flipped into the transverse plane, and the protons precess in-phase (depicted with one red vector in the circle). C) The protons start to precess out of phase, the longitudinal magnetisation starts to recover and transverse magnetisation decreases (depicted by the circle with multiple red vectors). D) Recovery of the longitudinal magnetisation is also referred to as T1 relaxation and disappearance of magnetisation in the transverse plane (T2 relaxation). This image is reproduced from a book written by Currie et al. [35]

increases, and the higher magnetic field is in the top of the skull. The precession frequency of the spins will vary depending on the gradient, and the RF-pulse needs to match this frequency to flip the spins into the transverse plane. Therefore, only the spins in the selected volume of interest will generate a signal.

Slice is selected with the slice selection gradient. The second step in spatial encoding is applying a frequency encoding gradient to alter the main magnetic field in the selected slice by changing the precessing frequency slightly more or less than the slice average. The final step of spatial encoding is phase encoding. In this step, the gradient is turned on for a short amount of time. During this time, the spins that are in the higher magnetic field will precess with a higher precession frequency than spins that are in the location with the lower magnetic field. When the phase encoding gradient is switched off the spins will start to spin with the
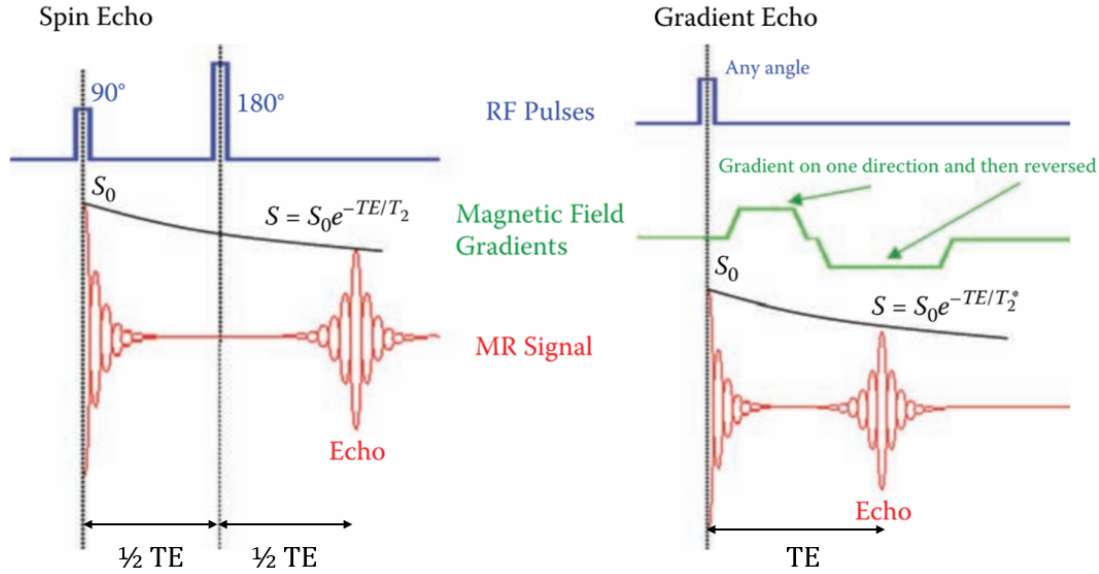
Fig. 4. Schematic illustration of the sequences of a spin echo and a gradient echo technique. In the equation S_0 is the signal after the RF-pulse, S is the decaying signal, TE is the echo time in ms, $T2$ is the T2 relaxation time in ms, and $T2^*$ is the $T2*$ relaxation time in ms. This figure is adapted from a book by Stroman et al. [37].

same precession frequency but maintain a different phase. The process of frequency and phase encoding is visualised in Figure 5.

The MRI collects the spatial frequency and phase information about every pixel in K-space. An image can be generated by performing a Fourier transform on the K-space. K-space is defined by the space covered by the phase and frequency encoding information [39]. The phase encoding allows you to go up and down in K-space, and the frequency encoding determines if you go right or left in K-space.

In this study, all patients undergo an MRI protocol with a T1, T2-weighted FLAIR (T2FLAIR), and BOLD scan. In the sections below, all three sequences will be explained.

2.2.1 T1-weighted scan

A T1-weighted scan is produced using short TE and TR times. The contrast and brightness of the scan will mainly be determined by the T1 properties of the tissue. A T1 scan is acquired with a gradient echo sequence. On Philips MRI scanners, this is called the Turbo Field Echo (TFE) sequence. In
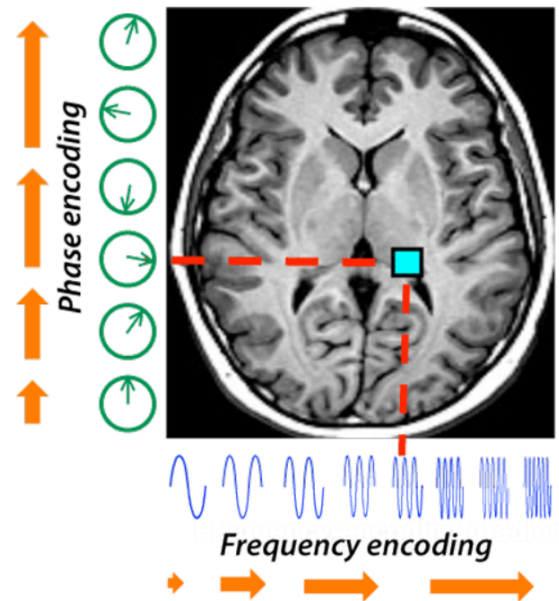
Fig. 5. Visualisation of the frequency and phase encoding to obtain spatial information. The spatial information of the blue voxel can be found with the specific frequency and phase difference at that location. This image is reproduced from Elster et al. [38]

7

Figure 6, the sequence and an example of a T1-
weighted image are shown. This sequence consists of an initial 180° pulse (inversion pulse)
followed by several rapidly acquired gradient echos that are obtained using a short TE and
small flip angles (α). The sequence uses a three-step cycle: 1) the inversion pulse to prepare
magnetisation for contrast control, 2) data acquisition with several rapidly acquired gradient
echos with a short TR and TE and a small flip angle (α), and 3) recovery of magnetisation
for additional contrast control [40]. The time between step 1 and step 2 is called the inversion
time (TI).
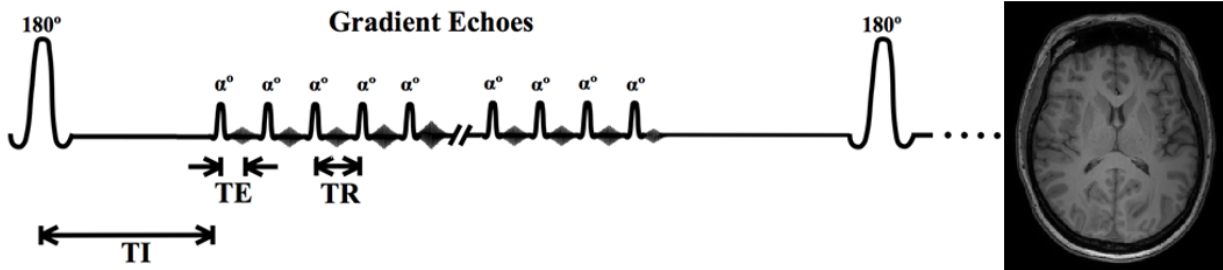
Fig. 6. TFE sequence of the T1-weighted MRI scan and an example slice of a T1-weighted
MRI scan

2.2.2 T2-weighted FLAIR scan

A typical T2-weighted scan is acquired with long TR and long TE times. The contrast and
brightness of the scan are predominantly characterised by the T2 properties of tissue. In these
images, cerebral spinal fluid normally gives a high signal because it has long T1 and T2 times.
However, in a T2FLAIR scan, an inversion pulse is given to remove the effects of these fluids
from the scan.
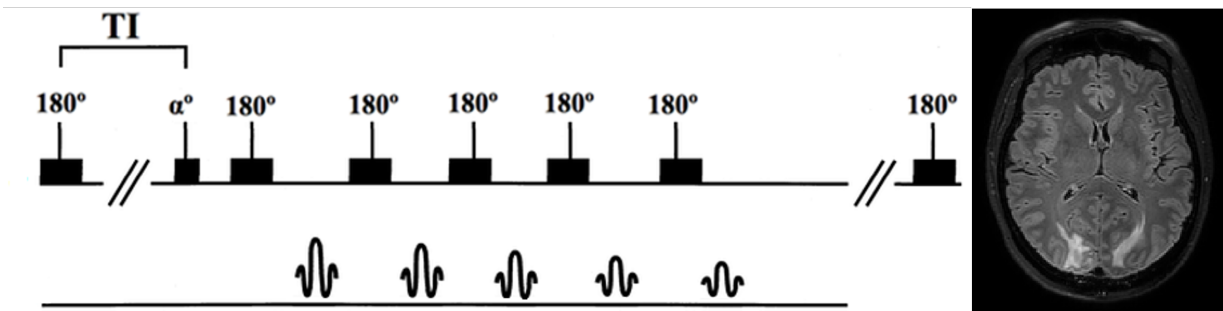
Fig. 7. TIR FLAIR sequence of the T2-weighted FLAIR scan and an example slice of a
T2FLAIR scan. The sequence starts with a 180° inversion pulse, followed by TI until the α
pulse and then followed by a fast spin echo sequence that is depicted as the train of 180° pulses
after the α pulse. In the line below, the obtained echoes are depicted. This Figure is reproduced
and adapted from the article by Ross et al. [41]. In the example of an T2FLAIR on the right,
oedema can be distinguished by the hyperintensities in the lower part of the brain.

The standard FLAIR sequence starts with a 180° RF inversion pulse to flip the longitudinal
magnetisation in the opposite negative direction. The net magnetisation in the negative lon-

gitudinal direction will return to the positive longitudinal direction while passing through the null value. After a specific TI, a 90° excitation pulse is applied to suppress liquids and measure the other tissues in the transverse plane. A typical TI to suppress water signal is approximately 2000 ms [42]. Nowadays, a fast spin echo sequence is used in combination with the inversion recovery sequence to speed up the acquisition time. An example of a fast T2FLAIR sequence and of an T2FLAIR image is given in Figure 7. On a Philips MRI scanner, this fast sequence is called the Turbo Inversion Recovery (TIR) FLAIR sequence.

2.2.3 Functional MRI scan

Functional MRI allows for the detection of changes in neural activity. This method is based on detecting the changes in blood flow and blood oxygen concentration in the brain. This change is also referred to as the blood oxygenation level-dependent (BOLD) signal change. The BOLD method depends on the difference in susceptibility between deoxygenated haemoglobin and oxygenated haemoglobin. Oxyhaemoglobin is diamagnetic, and deoxyhaemoglobin is paramagnetic. The magnetic property of haemoglobin changes when it loses oxygen, which alters the susceptibility of blood. Therefore, the signal is different depending on the levels of oxygen in the blood. [43]

The BOLD sequence is sensitive to changes in susceptibility of blood, which is caused by the difference in oxygen consumption and oxygen delivery. The ratio between oxygen consumption and oxygen delivery is the oxygen extraction fraction (OEF) and is defined in Equation 2. The changes in OEF will change the balance of oxygenated hemoglobin and deoxygenated hemoglobin, which depends on the cerebral metabolic rate of oxygen ($CMRO_2$), cerebral blood flow (CBF) and oxygen content (CO) in the blood [44].

$$OEF = \frac{oxygen\ consumption}{oxygen\ delivery} = \frac{CMRO_2}{OC \cdot CBF} \tag{2}$$

An active region of the brain will increase CBF to support that region with more oxygen. CBF increases much more than $CMRO_2$ and this will reduce the OEF. The signal of a BOLD scan is the reduction of OEF during an increase in neural activity [43]. If a vessel loses the ability to increase the CBF, the CBF and the $CMRO_2$ will stay equal. This leads to more deoxyhemoglobin and a lower BOLD signal in that area. This is how the change in BOLD signal could translate to vessel damage.

Echo Planar Imaging
Image acquisition of the BOLD scan is performed with echo planar imaging (EPI), which is a fast acquisition technique but has a limited spatial resolution. All lines in K-space are filled within one or more TRs. These TRs are referred to as shots, one TR is single-shot EPI, and more TRs is multishot EPI. The phase encoding and frequency encoding gradients are turned on and off very rapidly, to allow a fast filling of K-space (see Figure 8a and 8b) [42]. Figure 8c, shows an example of a BOLD image of one of the patients in this study.

The EPI technique can create several artefacts in the BOLD scan. An artefact that was visible in all the BOLD images of this study was the geometric distortion artefact. These distortions are caused by inhomogeneities in B_0 and inhomogeneities induced by other factors.
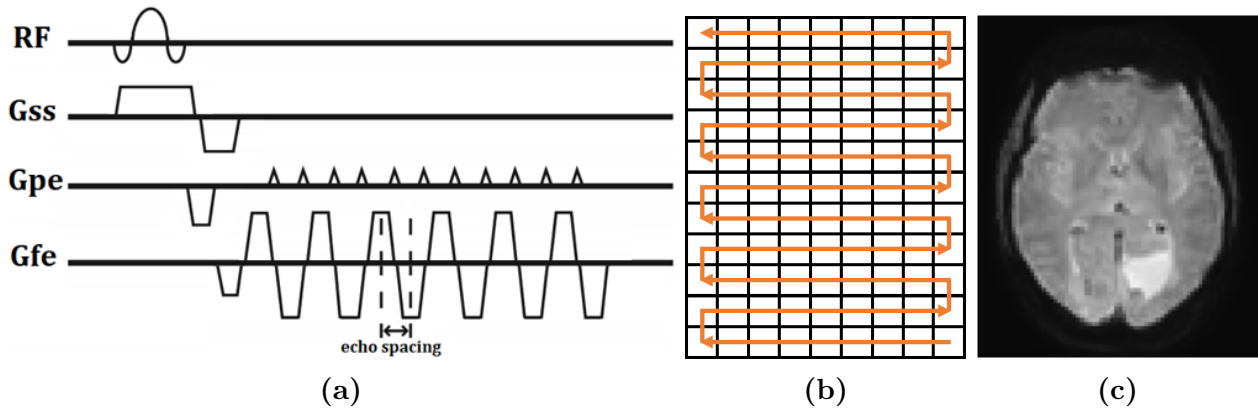
Fig. 8. Illustration of the gradient echo EPI sequence, the filling of K-space, and an example of a BOLD image. a) Shows the gradient echo EPI sequence where Gss, Gpe, and Gfe resemble the gradient for slice selection, phase encoding and frequency encoding, respectively. The echo spacing is the interval between two consecutive echoes. This image is reproduced and adapted from an article by Gianelli et al. [45]. b) Shows the filling of K-space during the sequence. c) Represents an example of a BOLD image of one of the patients from this study.

The inhomogeneities are particularly prominent on the interfaces between air and tissue, such as the skull base and the nose. In these areas, the protons feel a different magnetic field and start to precess in a different frequency. This leads to misplacement of signal and causes the geometric distortion artefacts in the image along the phase encoding direction [46]. In neuroimaging, this mostly leads to distortions in the front of the brain (see Figure 9) and at the base skull. This artefact can be minimised by performing multishot EPI but this will also increase the acquisition time.

Fig. 9. Illustration of the geometric distortion artefact that is common with the EPI technique.

2.3 Cerebrovascular Reactivity

As mentioned before, CVR is the ability of a blood vessel to dilate to respond to a vasoactive stimulus. The CVR of a blood vessel is measured with a cerebrovascular stress test, where the patient undergoes a breathing stimulus during a BOLD scan in the MRI scanner. In this study, patients receive a breathing stimulus delivered by a computer-controlled air blender that delivers a higher concentration of CO_2 to patients during the BOLD scan.

The vasoactive stimulus is delivered in a breathing protocol, where the baseline of the patient is measured for five minutes, afterwards, a block of CO_2 is administered, and subsequently, the baseline of the patient is measured again (see Figure 10). The computer-controlled air blender measures the level of CO_2 and O_2 in the exhaled air, which are referred to as end-tidal CO_2 or O_2 traces. The measured end-tidal traces closely resemble the arterial gas concentrations of CO_2 and O_2, and therefore, the end-tidal traces are a suitable surrogate for measuring the magnitude of the

vasoactive stimulus.

Fig. 10. Protocol of the breathing stimulus and an example of the breathing trace of one patient. The target depicts the targeted end-tidal CO_2 trace, and the breathing trace represents the measured end-tidal trace of CO_2. First, the baseline breathing traces of the patient is measured, then the block of extra CO_2 is given, and afterwards, the baseline is measured again.

This artificially increased concentration of CO_2 in blood has a vasodilating effect and also increases CBF [47]. In this case, the oxygen consumption ($CMRO_2$) stays equal, the vessel dilates to increase the CBF to supply the brain with a continuous supply of oxygen. This process increases the OEF and therefore also increases the BOLD signal [48]. If a vessel is not able to dilate anymore, for example, due to irradiation damage, the CBF is not able to increase in that area and the measured BOLD signal will be low.

2.4 Image Registration

In the study, data is obtained at different time points, with different scanning modalities and with multiple MRI sequences. All these scans are not in the same space due to the movement of the patient between sequences or pose differences in the baseline MRI, follow-up MRI, and computed tomography (CT) scanner. These scans need to have spatial correspondence to be able to compare them with each other. The images are aligned using image registration. Image registration determines the best geometric alignment between a reference image and a moving image. During the registration, the geometrical transformation is determined that maximises the similarity between the moving and the reference image. This geometric transformation is represented in a transformation matrix which needs to be applied to the moving image to register it to the reference image. During the registration with the transformation matrix, the moving image is resampled and will have the same field of view as the reference image.

Three types of transformations can be applied during registration and depend on the degrees of freedom (DOF). The following transformations will be discussed: rigid and affine registration. A rigid transformation has 6 DOF and can translate and rotate the image. The affine transformation has 12 DOF and can scale and shear the image in addition to the rigid transformations [49]. Another type is nonlinear (or nonrigid) registration, which has unlimited DOF and can cause tiny local changes in the to be registered image. This study does not use nonrigid transformation methods, and therefore, this will not be discussed further.

Cost functions are used to quantify and find the transformation that maximises the similarity between the moving and the reference image. There are different cost functions, some are based

on geometrically defined features within an image and others work on the intensity values in the images. The intensity-based cost functions are more reliable and accurate [50] hence these cost functions will be used in this study and discussed in the following section.

2.4.1 Cost Functions

Intensity-based cost functions can be divided into intra- and inter-modal functions. Intra-modal cost functions are least squares (leastsq) and normalised correlation (normcor) and can be used with images that are from the same modality or the same MRI sequence. Some inter-modal cost functions are mutual information (mutualinfo), normalised mutual information (normmi), and correlation ratio (corratio). These cost functions can be used between different MRI sequences and some also between different modalities. The definitions of the cost functions are listed in Table 1. In the equations, X and Y are the images that are being registered. In the following paragraphs, an explanation will be given of the five cost functions.

Table 1. The definitions of the intensity-based cost functions: leastsq, normcorr, mutualinfo, normii, and corratio. This table is adapted and reproduced from an article by Jenkinson et al. [51]

Cost function	Equation	Minimum	Maximum
leastsq	$\Sigma(Y - X)^2$	0	∞
normcorr	$\dfrac{\Sigma(X \cdot Y)}{\sqrt{\Sigma X^2}\sqrt{\Sigma Y^2}}$	-1	1
mutualinfo	$H(X,Y) - H(X) - H(Y)$	$-\infty$	0
normmi	$\dfrac{H(X,Y)}{H(X) + H(Y)}$	0	1
corratio	$\dfrac{1}{Var(Y)}\sum\limits_{k}\dfrac{n_k}{N}Var(Y_k)$	0	1

Least squares
The two images are being subtracted from each other. These values are squared to ensure a positive number to ensure that negative and positive values do not cancel each other out (see Table 1). The resulting value needs to be minimised to get the best image registration. This cost function is suitable for intra-modal images with the same sequence because this function can not manage large intensity changes between the images.

Normalised Correlation
This cost function calculates the correlation between the two images. The intensities are multiplied and mean intensity values are subtracted (see Table 1). The values of this cost function

need to be maximised to find the maximum correlation and optimal registration of the two images. This option is an intra-modal function and can manage linear intensity changes between two images. The images have to be generated with the same MRI sequence, e.g., a T1-weighted and T1-weighted scan with different contrast/brightness.

Mutual Information

The entropies of the individual images ($H(X)$ and $H(Y)$) is subtracted from the joint entropy of the images ($H(X,Y)$) (see Table 1). The results of this cost function need to be maximised to find the best image registration. With Equation 3 the entropy of X or Y can be calculated. In this equation, I can be image X or Y and $p(i)$ is the probability of a certain intensity in image X or Y. The joint entropy is calculated with Equation 4, where p_{ij} represents the joint probability distribution of image X and Y. Mutual information is calculated with distributions and allows registering images from multiple modalities.

$$H(I) = - \sum_i p_i \log p_i \tag{3}$$

$$H(X,Y) = - \sum_{ij} p_{ij} \log p_{ij} \tag{4}$$
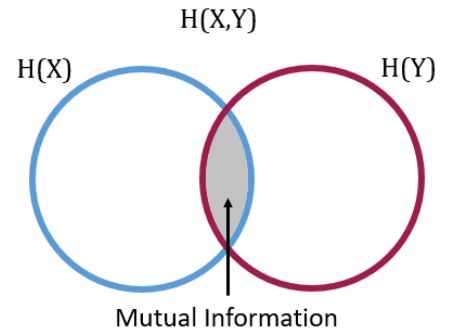
Fig. 11. Visualisation of entropy and shared mutual information. The blue circle is the entropy of X ($H(X)$), the red circle is the entropy of Y ($H(Y)$) and both circles together are the joint entropy of X and Y ($H(X,Y)$). The shared grey space is the mutual information where both circles are overlapping.

Normalised Mutual Information

This cost function normalised the mutual information to scale the results between 0 (no correlation) and 1 (highest correlation) is the normalised version of mutual information. The joint entropy is divided by the summed $H(X)$ and $H(Y)$. This cost function can be used to register inter-modal images.

Correlation Ratio

Correlation ratio measures the functional dependence between X and Y, where 0 is no functional dependence and 1 is high functional dependence. The functional dependence is a relationship between two features such as the intensity and the position. [52] In the equation in Table 1, the variance is calculated of Y and Y_k. Y_k is the kth set defined as a set of intensities in image Y at positions where the intensity in
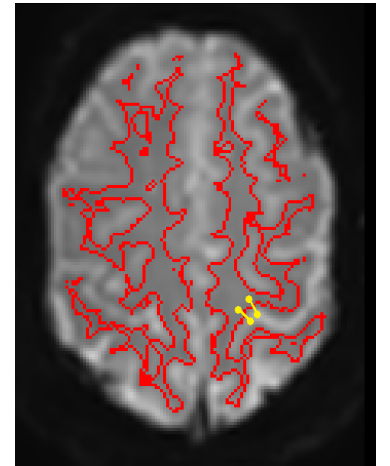
Fig. 12. Illustration of the BBR cost function. The red segmentation is the WM segmentation and the yellow dots represent a sample at either side of the segmentation.

13

X is in the kth intensity bin of the histogram. This cost function is also able to be used for inter-modal registrations but preferably between MR modalities [53].

Boundary-Based Registration
This cost function is specially created for scans that were generated with the EPI technique. The input is a T1 scan, a WM segmentation of the T1, and an EPI scan with grey-white intensity contrast. The WM segmentation is overlapped with the EPI image and then samples are taken at a distance from either side of the segmentation. The intensity difference between the two samples needs to be large to have a good registration. This boundary-based registration (BBR) only uses samples at either side of the WM segmentation [54]. This process is visualised in Figure 12.

2.4.2 Interpolation Methods

When the moving image is registered to the reference image, the matrix of the moving image does not match up perfectly with the reference image. To match the matrix of the registered moving image, interpolation is needed to fill in values between the grid points. This process is visualised in Figure 13, where the white grid is the original image and the yellow grid is the registered image. The value of the yellow dot in the grid needs to be determined, which is calculated with interpolation functions such as nearest neighbour (NN), trilinear and spline interpolation [53].

(a) Nearest Neighbour   **(b)** Trilinear   **(c)** Spline
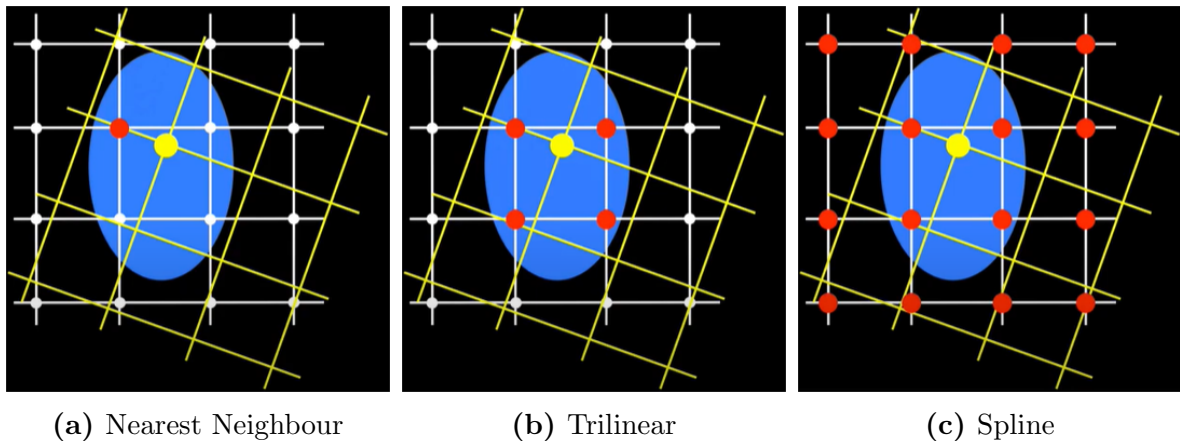
Fig. 13. Illustration of three interpolation techniques: a) NN selects the closest grid point, b) Trilinear selects the surrounding grid points and calculates a weighted average, and c) Spline includes more surrounding points to determine the value of the yellow dot. The original image is represented with the white grid and the registered image is represented with the yellow grid. The value of the bold yellow dot needs to be determined. This value is calculated with the selected grid points shown in red. This figure is reproduced from the FSL course by FMRIB [53]

Nearest Neighbour
Figure 13a, represents NN interpolation, this method finds the nearest white grid point (highlighted in red) and copies this value to the yellow grid point. This method is fast and it does not

create new values, only the values that were already in the original image are copied. Images that are interpolated with this method have 'blocky' edges and can look more pixelated than the original image. [53, 55].

Trilinear
This is a linear interpolation technique that is applied in three dimensions. For 2D images, this function is referred to as bilinear. This method is shown in Figure 13b, where the surrounding white grid points are selected (highlighted in red) and a weighted average of those points is calculated to define the yellow grid point. The average is weighted according to the distance of the red points to the yellow grid point. This method is quite fast but can also slightly blur the image. [53, 55].

Spline
This interpolation method includes even more points around the yellow grid point, to determine the value of the yellow dot in Figure 13c. This method creates sharper images and is good for modelling larger boundaries, and the interpolated image will look similar to the original image. The downside of this method is that it does not constrain the limits of the output and can create values that were lower or higher than the maximum or minimum of the original image. If the image has artefacts or if the patient has abnormalities, these abnormalities can be spread out with a spline interpolation method [53, 55].

Interpolation methods are never perfect and change the original image. Interpolation adds artificial values to the data and this results in values that were not exactly measured during the scan. Therefore, the number of interpolations performed on an image should be minimised. If an image needs to be registered multiple times then the transformation matrices can be combined to perform one resampling step [53].

3   Methods

This thesis is reporting the data of the APRICOT (Assessing and Predicting Radiation Influence on Cognitive Outcome using the cerebrovascular stress Test) study that is carried out at the University Medical Center (UMC) Utrecht. The APRICOT study investigates the relationship between baseline CVR and changes in cognitive test results for patients with BM at baseline and three months after RT (follow-up).

All included patients of the APRICOT study were also included in this thesis. All patients have BM and received SRS as part of their treatment plan. One to two weeks before irradiation treatment, each patient underwent a CT scan. This CT scan was used to delineate tumours and organs at risk and plan the dose distribution of the irradiation treatment plan. On the same day, but before their irradiation treatment, all patients underwent the MRI scan with the breathing stimulus. Three months after irradiation, all patients came back for the follow-up and underwent the same MRI scan with the breathing stimulus. The journey of the patient during the APRICOT study is depicted in Figure 14.

All acquired scanning data of each patient was anonymised and given an APRICOT patient code (e.g., APP003 for the third included patient). The baseline scanning data is stored in a folder with the APRICOT patient code name. The follow-up data is stored in a separate folder named the APRICOT patient code with an added 'b' to avoid confusion (e.g., baseline stored in folder 'APP003', and follow-up stored in 'APP003b').
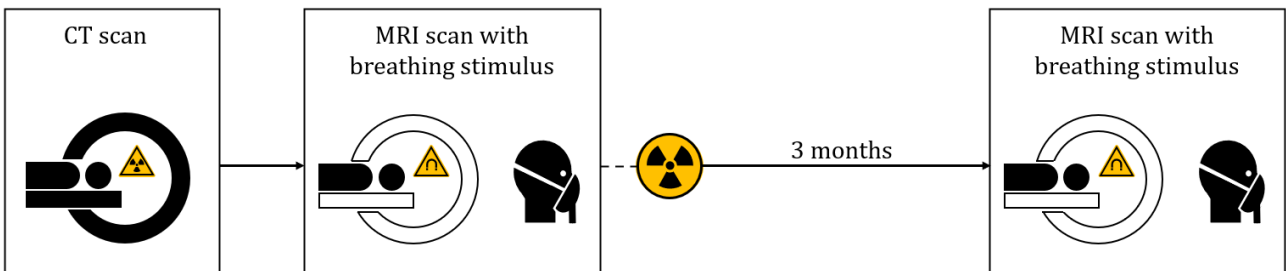
Fig. 14. Overview of the journey of each patient. The first block depicts the CT scan that each patient underwent before irradiation treatment. One or two weeks after the CT scan, the patient underwent an MRI scan with a breathing stimulus which is shown in the second block. The radiation sign depicts the irradiation treatment that patients receive on the same day as their first MRI scan. Subsequently, three months after irradiation treatment, the patient underwent the same MRI sequence with the breathing stimulus.

3.1   Ethics

The APRICOT study was carried out under the research protocol of the APRICOT study with the METC (Medical Ethics Review Committee) number: 18-747. The APRICOT study was conducted in accordance with the principles of the Declaration of Helsinki (64th WMA General Assembly, Fortaleza, Brazil, October 2013) and according to the WMO Act (Medical Research Involving Human Subjects Act).

All potential participants had an appointment with one of the researchers of the APRICOT study, where they received information about the study and had the chance to ask questions

regarding the study. The patients had three days to consider if they wanted to participate in the APRICOT study. If the patient decided to participate, an appointment for the MRI scan was scheduled on the same day before their RT appointment. Before the MRI scan, the informed consent was signed by the patients.

3.2   Patient Inclusion

In total, 15 patients were enrolled in the APRICOT study. Two patients had to be excluded because the breathing challenge could not be finished (APP004), or there were too many artefacts in the BOLD scan (APP002). Five of the residual 13 patients underwent the follow-up scan at this moment. The follow-ups of the other patients will be performed after the conclusion of this thesis. Additional relevant clinical information about the patient is given in Appendix A.

3.3   CT acquisition and pre-processing

The CT data was obtained from the clinical radiotherapy servers of the UMC Utrecht in the Netherlands. For each patient, the dose distribution was recalculated into an equivalent dose distribution per 2 Gy fractions (EQD_2). Subsequently, masks of the BM were created with the delineated tumours. A more detailed explanation of the EQD_2 calculation and the creation of the tumour masks is given in Appendix B. After collecting the CT data (CT scan, tumour mask, and dose distribution), the data was transferred to the research servers of UMC Utrecht.

3.4   MRI Acquisition and breathing stimulus

MRI data was obtained with a 3 Tesla MRI scanner (Philips Medical Systems, Best, The Netherlands) using a 32-channel head coil. The MRI scanning protocol for this study contained a T1, T2FLAIR, and 17 min long BOLD scan. In Appendix C, the MRI acquisition parameters are given. The patients underwent the same scanning protocol before and three months after their irradiation treatment.

The MRI data was directly saved on the research server of the UMC Utrecht after scanning the patient. The MRI scanner is a Philips scanner that stores the data in a PAR and a REC file. The PAR file is a text file that contains the scan parameters and the REC file contains the actual scanning data. These PAR/REC files were converted to NIfTI format with the *dcm2niix* convertor.

In order to make the CVR maps, the patients had to undergo a breathing stimulus during the BOLD scan. This stimulus was delivered to the patients with a computer-controlled gas blender (RespirAct™, Thornhill Research Institute, Toronto, Canada). The RespirAct is able to deliver precise and repeatable changes in oxygen and carbon dioxide concentrations in arterial blood. The amount of carbon dioxide and oxygen that is dissolved in blood is also referred to as PCO_2 (partial pressure CO_2) and PO_2(partial pressure O_2), respectively. During the stimulus the Respiract targets to increase of end-tidal PCO_2 with a 10 mmHg above the patient's baseline value.

Prior to the MRI scan, the patients were fitted with a facemask that was later attached to the RespirAct. Tegaderm™ film was used to stick the facemask to the patient's face and to assure gasses could not leak out. During the entire MRI protocol, the patient's PCO_2 and PO_2

were measured by the RespirAct [56]. In Figure 10 of Section 2.3, the breathing protocol is shown together with an example of the measured end-tidal PCO_2 of a patient.

3.5 Development of Analysis Pipeline

All obtained scans need to be brought into spatial correspondence to be able to compare the baseline CVR with the follow-up CVR. This was executed with an image analysis pipeline that registers the data to the baseline T1 scan. The following sections will describe the process of the development of this pipeline. The data that needed to be registered by this pipeline is a baseline CT scan with dose distribution and tumour mask, baseline BOLD scan, baseline T2FLAIR scan, follow-up T1 scan (T1b), follow-up T2FLAIR (T2FLAIRb), follow-up BOLD (BOLDb). The pipeline is created using one ideal patient (APP003) with scanning data with no artefacts and sufficient breathing traces during the breathing stimulus. In Figure 15, the data that is acquired for each patient is visualised. In the following sections, the development of the pipeline is discussed shortly, and in Appendix D a more detailed explanation can be found.
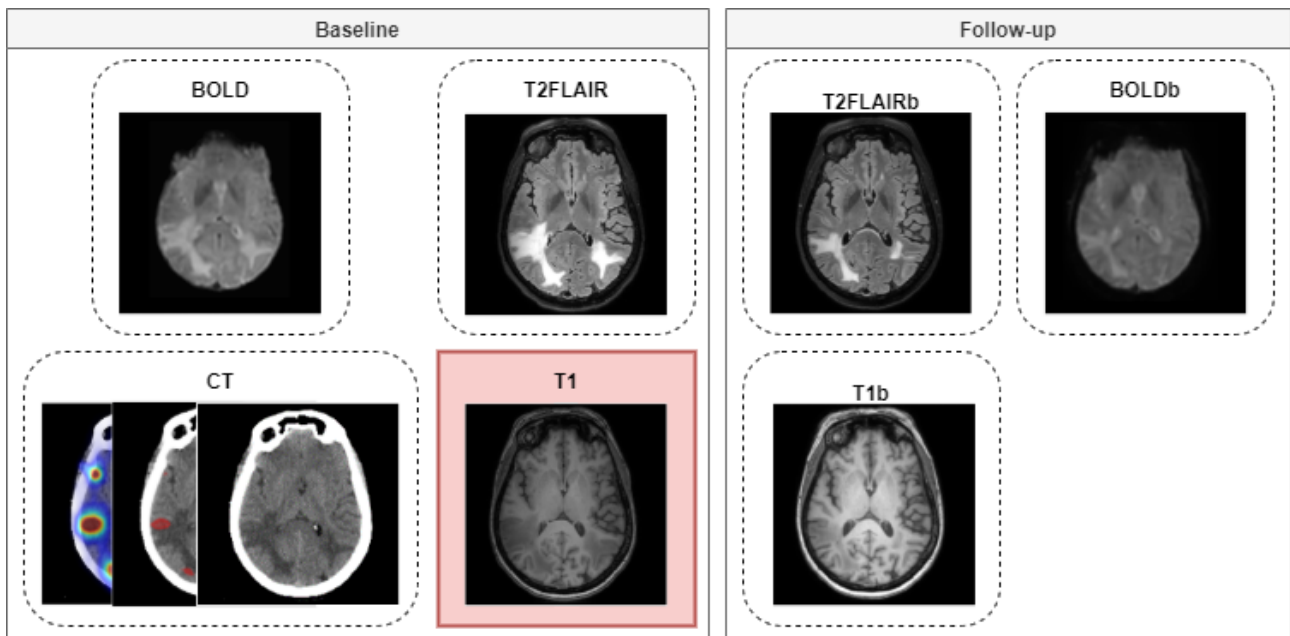
Fig. 15. The data that is acquired of each patient. The left side shows the baseline scans and the right side shows the follow-up scans. All the scans need to be registered to the T1 scan, this is depicted with the red square.

The pipeline was built on the research server of the UMC Utrecht and consists of two separate bash scripts, one for baseline and one for follow-up data. The pipeline makes use of FSL (The Analysis Group, FMRIB, Oxford, UK.), which is a library of analysis tools for brain imaging data. The bash scripts of the baseline and follow-up registration pipeline can be found in Appendix G.

All scans need to be registered to one reference scan, ideally, this scan has the best resolution and contrast of all scans [53]. The CT has the best resolution, and the T1 and T2FLAIR have

the best contrast. The T1 scan was selected as the reference image, this scan has good contrast and the image intensities are more relatable to the CT scan in comparison with the T2FLAIR. E.g., the intensity of the ventricles of the brain and oedema in CT and T1 are both lower than brain tissue. This might make the registration of CT with an MRI scan easier. Prior to the registration of the anatomical MRI scans (T1, T1b, T2FLAIR, and T2FLAIRb), the brain in each scan was extracted using FSL BET(Brain Extraction Tool). The extracted brains are registered to each other, which helps the registration tool to focus on the registration of the brain and not the surrounding tissue.

For every registration the cost function, DOF and interpolation method needs to be selected. The ideal parameters were selected by performing the registration multiple times with the applicable cost functions and rigid (6 DOF) and affine (12 DOF) registration. The results were visually analysed using ITK-SNAP, and the best option was selected. The interpolation method was selected based on the type of data and the function of that scan in the data analysis.

3.5.1 Baseline Registration Pipeline

This part of the pipeline needs to register all the baseline data, CT scan with dose distribution and tumour mask, T2FLAIR scan, and BOLD scan. The following paragraphs will describe how the different scans were registered to the T1 scan. A flowchart of the baseline pipeline can be seen in Figure 16. A more detailed description of every baseline registration can be found in Appendix D

CT registration
The CT registration was performed using FSL FLIRT (FMRIB's Linear Image Registration Tool). This function is a fully automated function in FSL for rigid and affine registration [51,57]. The CT to T1 coregistration is inter-modal and requires an inter-modal cost function. The inter-modal cost functions that are available for FLIRT are corratio, mutualinfo, and normcorr. The cost function normmi, gave the best result and was selected as the cost function for the CT to T1 registration. The CT registration was performed with affine registration and trilinear interpolation. The resulting transformation matrix was used to register the tumour mask and dose distribution to the T1 scan with NN interpolation.

T2FLAIR Registration
As mentioned before, the brains of the anatomical scans (T1 and T2FLAIR) were extracted before registration. The registration was first performed with both extracted brains and afterwards, the whole T2FLAIR scan was registered to the T1 scan. The intensities of T1 and T2FLAIR are different and therefore the applicable cost functions were corratio, mutualinfo, and normmi. Leastsq and normcorr are not sufficient for these intensity differences.

All three cost functions registered the T2FLAIR sufficiently, and no differences between the scans could be observed. The cost function normmi was selected arbitrarily. The affine registration resulted in a T2FLAIR that was scaled down in comparison to the T1 scan. The rigid registration gave optimal results and was selected for the baseline T2FLAIR registration. Trilinear was selected as the interpolation method.
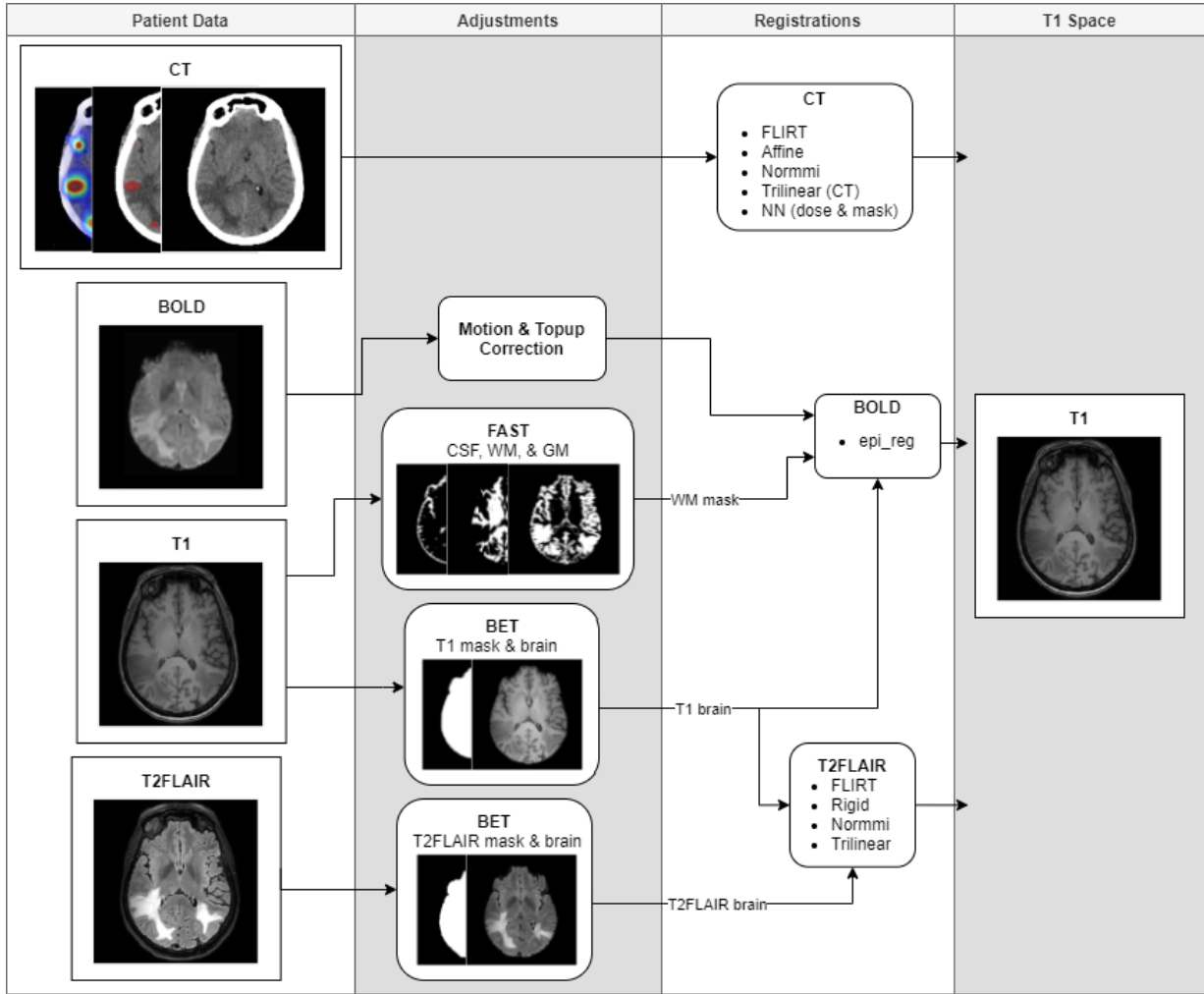
Fig. 16. Flowchart of the baseline image registration pipeline. The CT scan, BOLD scan, and T2FLAIR scan need to be registered to the T1 space. The CT data can be registered directly without any adjustments. The T1 is segmented into a CSF, WM, and GM mask, and the brain is extracted. The BOLD image is corrected for motion and the geometric distortion artefact. Subsequently, the WM mask and extracted brain of T1 is used to register the BOLD to T1 space. The T2FLAIR brain is extracted and together with the T1 brain, the T2FLAIR is registered to T1 space.

BOLD registration

At first, there were some difficulties with the registration of the BOLD scan to the T1 scan. The edges of the BOLD scan could not line up with the T1. This problem was caused by the geometric distortion artefact that is explained in Section 2.2.3. This artefact is removed using FSL function topup, which creates a coefficient correction field that can be used to correct the BOLD scan [58, 59]. The process of FSL topup is explained in Appendix D.

The registration of the BOLD scan to baseline T1 space is achieved with the FSL function epi_reg. This function is a specialised FLIRT function specially made for EPI images and uses the BBR cost function that was discussed in Section 2.4.1. Epi_reg was run with the T1 scan, BOLD scan, field correction of the topup, WM segmentation, echo spacing, and phase

encoding direction to perform this registration. The WM segmentation was generated with FSL FAST (FMRIB's Automated Segmentation Tool), and this function segments a 3D brain scan into three different tissue types (GM, WM, and CSF) [60]. The registration parameters of epi_reg cannot be specified and are already predefined. The epi_reg function uses the BBR cost function, rigid registration, and spline interpolation.

3.5.2 Follow-up Registration Pipeline

In this section, the development of the follow-up registration pipeline is discussed. As mentioned before, the patient does not undergo a second CT scan during the follow-up. Therefore, this developed pipeline needed to register the BOLDb, T2FLAIRb and T1b scan to the baseline T1 scan. The interpolation method trilinear was selected for all MRI scans, and NN interpolation was selected for categorical masks such as a WM or GM segmentation. An overview in the form of a flowchart is given in Figure 17. The development of the follow-up registration pipeline is discussed in more detail in Appendix D.

T1b Registration
Before registration, the brain was extracted from the T1b scan using FSL BET. This registration is an intra-modal registration and can be performed with leastsq and normcorr. The T1b scan of the test patient has some intensity differences between the T1 and T1b scan. Therefore, the cost function normorr is selected for this registration. Rigid registration is performed because affine registration slightly shrunk the T1b scan. Trilinear was used as the interpolation method.

T2FLAIRb Registration
The brain of the T2FLAIR scan is also extracted prior to the registration with FSL BET. The registration of T2FLAIRb needed to be performed with a cost function that can manage intensity differences such as mutualinfo, normmi, and corratio. The cost function normii was selected for this registration. Again, trilinear interpolation is used during this rigid registration.

BOLDb Registration
Before registration to T1 space, the BOLDb is corrected for the geometric distortion artefact. The same process with FSL topup is used as described in the paragraph about the BOLD registration (Section 3.5.1) to remove the distortions.

Two options were considered for this registration. The first option uses the epi_reg function to register the BOLDb directly to T1 space. The downside of this option could be that it would be sensitive to changes in the brain of the patient at follow-up in comparison to the baseline scans. An example can be seen in Figure 15, where the follow-up T2FLAIR scan clearly shows less oedema than the baseline T2FLAIR scan of APP003. The second option is to divide the registration into three steps: 1) register BOLDb to T1b with epi_reg, 2) multiply this transformation matrix with the transformation matrix of T1b to T1 registration and 3) use the combined matrix to directly register the BOLDb to the T1 with normii and spline as the interpolation method.

The WM segmentation for registration with epi_reg in the first step of option two is generated with FSL FAST.Both options resulted in a similar registration, the second option was selected since it is less sensitive to changes in the anatomy in the follow-up scans.
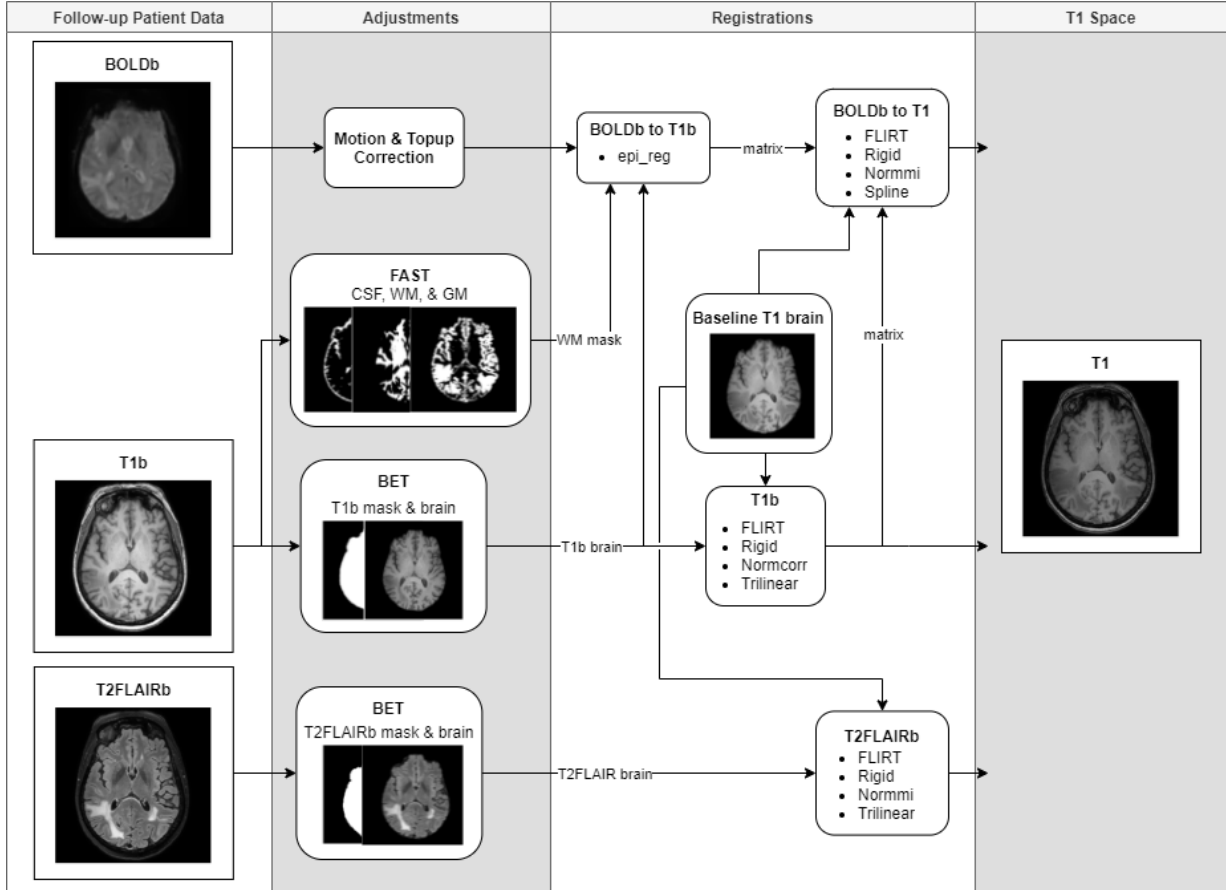
Fig. 17. Flowchart of the follow-up image registration pipeline. The T1b scan, BOLDb scan, and T2FLAIRb scan need to be registered to T1 space. The T1b and T2FLAIRb first undergo brain extraction and are then registered to T1 space with the baseline T1 brain. The T1b is also segmented and divided into a CSF, WM, and GM segmentation using FAST. The BOLDb scan is corrected for motion and the geometric distortions, and afterwards, registered to the T1b using the T1b WM segmentation and T1b extracted brain. The matrix of the T1b to T1 registration is multiplied with the matrix of BOLDb to T1b. This combined matrix is used to directly register BOLDb to T1.

3.5.3 CVR calculation

The CVR calculation was performed in BOLD space to obtain the baseline CVR map and in BOLDb space to obtain the follow-up CVR (CVRb) map. The CVR map calculation is executed with the seeVR toolbox (seeVR, Utrecht, The Netherlands) [61]. The CVR maps are generated with the BOLD motion correction parameter, tracked end-tidal CO_2 trace, and segmentations of WM, GM, and CSF. In the paragraphs below, the calculation of the CVR maps will be explained

First, data points that are three standard deviations above the end-tidal CO_2 trace are considered outliers and removed from the breathing trace. Secondly, the BOLD data and end-tidal CO_2 trace are aligned with each other. The CO_2 block in the end-tidal CO_2 trace is selected, and the same block is selected in the BOLD data. This selected part of the end-tidal

CO_2 trace will now be referred to as the regressor.

Some blood vessels might dilate slower or are less sensitive to CO_2 than other vessels, and for these vessels, the end-tidal CO_2 might not provide an accurate model for the CVR calculation. Hemodynamic response functions (HRF) are used to model the dispersion of the signal that might be present in some of these vessels inside the brain. The HRF is convolved with the regressor to take into account the slower or less sensitive vessels.
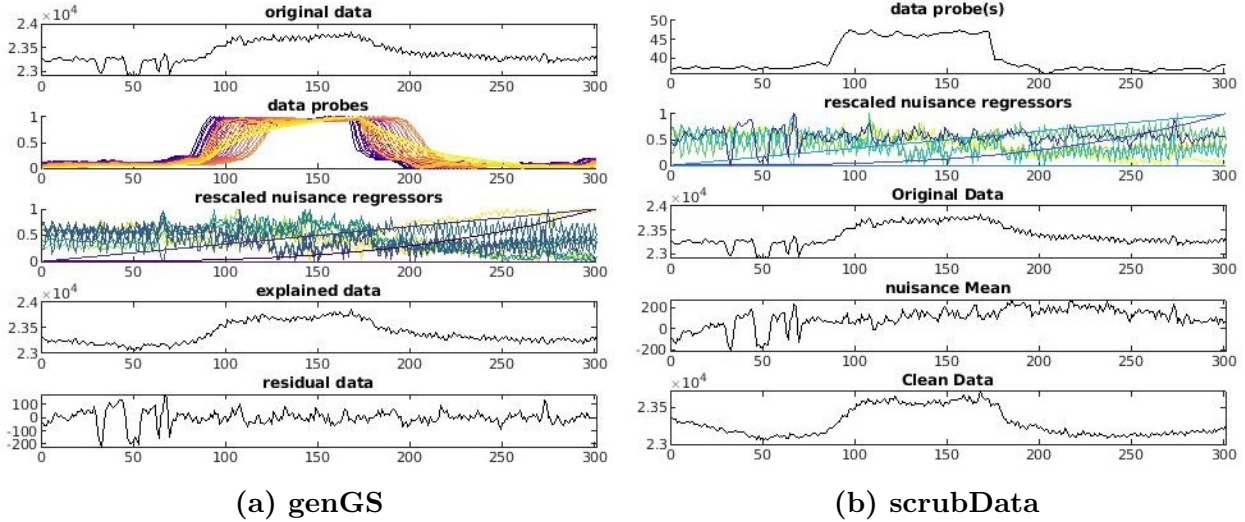
(a) genGS   (b) scrubData

Fig. 18. Visualisation of the functions genGS (a) and scrubData (b). Figure a shows the BOLD data (original data), HRF convolved with the regressor (data probes), rescaled nuisance regressors, explained data and residual data. The nuisance regressors and regressors are used to explain the original data. The nuisance regressors that could not be explained in the original BOLD data are taken into one new parameter, the residual data. Figure b shows the breathing trace (data probe), rescaled nuisance regressors with residual data included, original BOLD data, nuisance mean, and original data with the nuisance mean subtracted (clean data).

Thirdly, a new parameter is generated, the nuisance regressors. The nuisance regressors represent factors that could have influenced the BOLD data. The motion correction and Legendre polynomials are included in the nuisance regressors. The Legendre polynomials correct for drift caused by the scanner that is heating up during the acquisition. The drift can be characterised as signal degradation and intensity changes in the scan. The function called genGS is used to take the information of the nuisance regressors and regressor to explain the BOLD data. The BOLD data that could not be explained with the convolved HRF data probes and nuisance regressors is summed up into one new parameter, the residual data. This process is shown in the graph in Figure 18a. The residual data is also included in the nuisance regressor.

Afterwards, the nuisance regressors are used to clean up the BOLD data with the function scrubData. The mean of the nuisance regressors is subtracted from the BOLD data to end up with a 'cleaned' version of the BOLD dataset (see Figure 18b). Finally, a linear regression is executed with the original end-tidal CO_2 regressor against every BOLD voxel. This means that the regressor is plotted against the BOLD voxels, and a line is fitted through it. The slope of the fitted line is the CVR in percentage BOLD change per mmHg CO_2.

CVR Registration

The CVR calculation with the seeVR toolbox needs as input the end-tidal CO_2 traces of the patient, BOLD scan, BOLD brain mask, and CSF, WM, and GM segmentation. The masks and BOLD scan all need to have the same spatial correspondance. Additional registrations were performed using the transformation matrices of the image registration pipeline. The BOLD to T1 matrix is inversed to register the CSF, WM, and GM segmentations from T1 space to the BOLD space. The brain mask of the BOLD was created with FSL BET that extracts the brain and generates a mask of the brain. The same process was performed for the follow-up scans. In Figure 19, a flowchart depicts the steps that were performed before the CVR calculation.
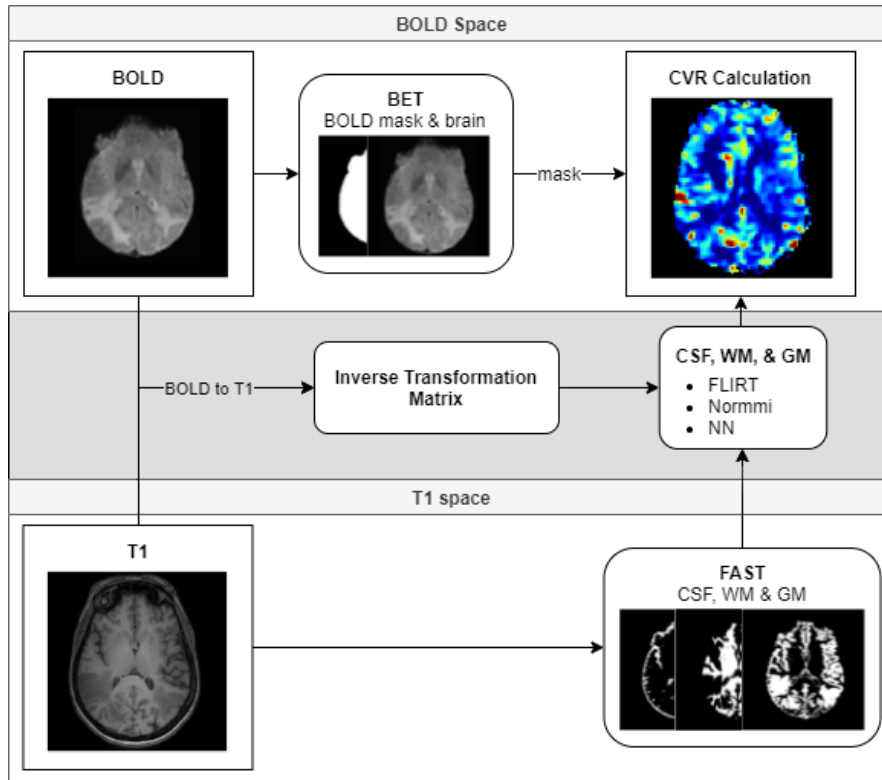
Fig. 19. Flowchart of the steps before the CVR calculation. The transformation matrix of BOLD to T1 is inversed to be able to register the CSF, WM, and GM segmentation to BOLD space. A BET is performed on the BOLD to generate a brain mask. The CVR calculation is performed with the brain mask, BOLD scan, breathing traces and CSF, WM, and GM segmentations. The same process is repeated for the follow-up CVR calculation.

3.5.4   Additional Registration for Data Analysis

The data analysis of the CVR maps is performed in baseline BOLD space. The considerations that led to this decision are discussed in Section 3.6. To perform the analysis, some scans or segmentations needed to be brought into baseline BOLD space. These scans were the dose distribution, tumour mask, CVRb map, and CSF, WM, and GM segmentation. The steps that were needed to register these are visualised in the flowchart of Figure 20.

Preferably, the data analysis always needs to be performed with the original data. In the case of this study, this would mean that the original BOLD and BOLDb data are used to calculate the CVR maps and that the CVR maps should not be interpolated. However, to perform the BOLD registration, the BOLD needed to be corrected for geometric distortions and additionally the data analysis of the CVR maps needed to be executed in the same space.

The corrected BOLD scans were used to calculate the CVR maps. It could be argued that the original BOLD data is not used for this calculation and that this makes the CVR maps less reliable. Conversely, if the corrections were not executed then the data in these distorted areas would have been built up, especially in the front of the brain. This would also have resulted in artefacts in these regions which would also make the CVR maps less reliable. The decision is made to calculate the CVR maps with the corrected BOLD to have fewer artefacts in the CVR maps.
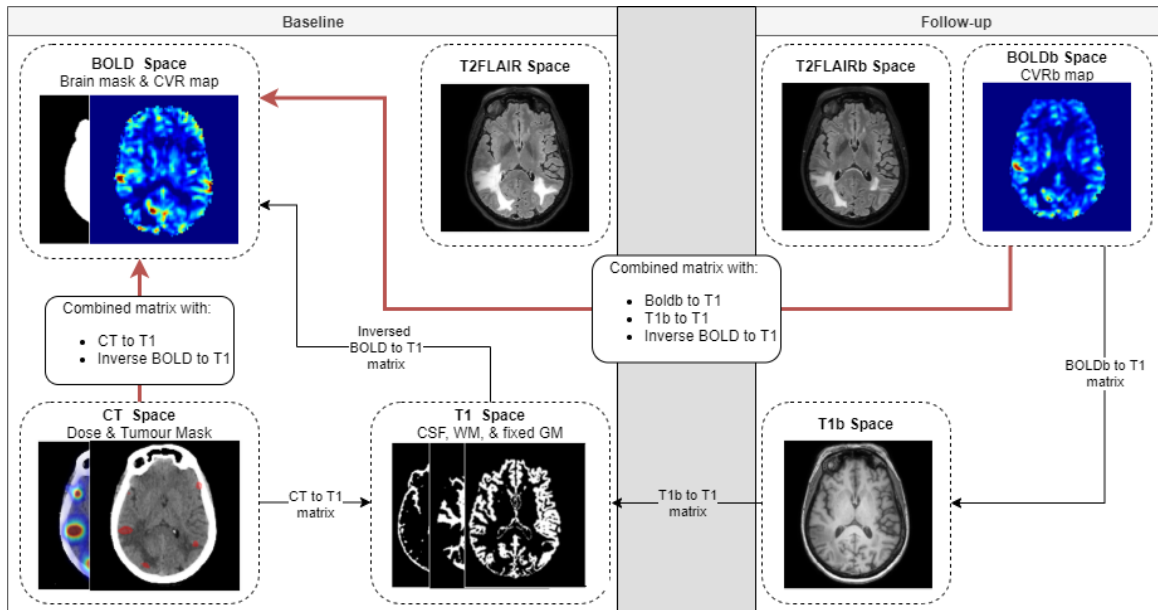
Fig. 20. Flowchart of the registrations that were needed to perform the CVR analysis in baseline BOLD space. This analysis needed the dose distribution, tumour mask, CVRb map and CSF, WM, and GM segmentations to be registered to baseline BOLD space. The registrations were accomplished by using the transformation matrices of the baseline (Fig. 16) and follow-up pipeline (Fig. 17). The red arrows depict the combined matrices that were combined for the analysis. The black arrows depict the registrations that were performed in the baseline or follow-up pipeline.

To know the location of the tumour and the dose distribution in the brain, the dose map and the tumour mask needed to be resampled into baseline BOLD space. This is accomplished by resampling the tumour mask and dose distribution with a combined transformation matrix. This matrix is created by multiplying the inversed transformation matrix of the BOLD to T1 registration with the transformation matrix of CT to T1 registration. The data analysis was performed separately for the WM and GM to determine the CVR in these different types of tissues. As mentioned in Section 2.1, GM consist of more blood vessels and therefore most of the response is expected to come from GM. The CSF, WM and GM are resampled to BOLD

space with the inversed BOLD to T1 transformation matrix.

Finally, to compare the baseline CVR with the follow-up CVR, CVRb needs to be in spatial correspondence with the baseline BOLD scan. This means that CVRb needs to be interpolated, which induces some uncertainty into the CVRb map. This registration is accomplished by combining the BOLDb to T1, T1b to T1, and inversed BOLD to T1 transformation matrices. The interpolation method that is used is NN to ensure that all CVR values stay equal and no artificial values are introduced into the data. Trilinear and spline interpolation interpolates between values, which results in artificial values that were not in the data set before interpolation.

3.6 Data Analysis and Statistics

With an in-house written script using MATLAB, data analysis was performed with the baseline and follow-up data. A VOI-based analysis is performed on the baseline data and a dose-based analysis is performed to compare the follow-up data to the baseline data after irradiation. The analysis for both methods was executed in baseline BOLD space instead of baseline T1 space. The MATLAB scripts that were developed for the creation of the segmentations and the calculation of the average CVR in the segmentations can be found in Appendix H.

When a moving image is registered to the reference image, it will be resampled into the field of view of the reference image. In this case, the matrix of the T1 scan is much larger (240x240x180) than the matrix of a BOLD scan (51x96x96). The resampling would create many more CVR values than that were originally in the CVR maps. For this reason, the decision was made to perform the analysis in BOLD space.

For the VOI-based analyses, VOIs around the tumour were created that expand with 2 to 14 pixels from the tumour. For the dose-based analysis, the treatment dose was divided into sections of <5 Gy, 5-8 Gy, 8-12 Gy, 12-16 Gy, and $\geq$16 Gy. These specific dose groups were selected after a discussion in the research group with a radiation oncologist. The reasoning behind this is that most of the change will happen close to the tumour which receives at least more than 16 Gy, and the least expected change is in the tissue that received less than 5 Gy. Other values were chosen in between these two dose values. An example of the VOI- and dose-segmentation of APP003 is given in Figure 21. Both segmentations were divided into WM and GM segmentation to find the average CVR in each type of tissue of the brain.

3.6.1 WM and GM Segmentations

The WM and GM segmentations were created in the registration pipeline using FSL FAST described in Section 3.5.1 and 3.5.2. The function automatically creates a GM, WM, and CSF segmentation. However, most of the patients in this study have regions with abnormal anatomy due to BM and oedema. For these patients, FAST includes oedema in the GM segmentation. A real GM mask is created by extracting an oedema mask from the GM segmentation. This oedema mask was made for each patient separately with a semi-automatic method using LST (Lesion Segmentation tool) and ITK-SNAP. LST is an open-source toolbox in SPM (Statistical Parameter Mapping Software, University College of London, UK) that automatically segments lesions using a T1 and T2FLAIR scan [62]. The false positives and false negatives from the LST segmentation were manually adjusted using ITK-SNAP. In Appendix E, an explanation is given on how the segmentations were generated.
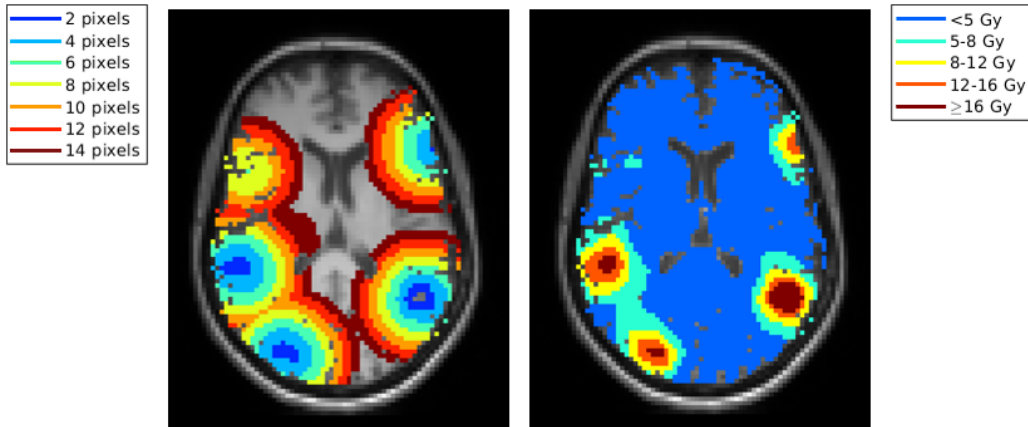
Fig. 21. Illustration of the segmentations of the VOI-based (left figure) and the doses-based (right figure) analysis. For illustrative purposes, each VOI around the tumour and dose section is given a different colour.

Oedema in the GM segmentation by FAST was corrected by extracting the oedema mask from the GM segmentation to create a real GM segmentation. This new GM segmentation was used to divide the VOI- and dose-based segmentations into a WM and real GM segmentation. There is no expected response from CSF since it does not contain cerebrovasculature, therefore, CSF was removed from the VOI- and dose-based segmentations. The brain tumours were also removed in both segmentations because the interest is in the reactivity of the cerebrovasculature and not in vessels inside the BM. Subsequently, the segmentations (VOI- and dose-based) are divided into GM and WM segmentations.

3.6.2 Statistical Analysis

The statistical analysis was performed using IBM SPSS Statistics for Windows, Version 27.0. (Armonk, NY: IBM Corp.). The statistical significance was set at a p-value of equal or less than 0.05. To assess the VOI-based results, a non-parametric repeated measures ANOVA (Friedman test) was used. In addition, a Wilcoxon signed-rank test was used to assess the differences between two VOIs (the VOI closest to the tumour and the VOIs at a distance). The results of the dose-based analysis were assessed with 1) a Wilcoxon signed-rank test to test if the difference per dose groupe between baseline and follow-up groups was significant, 2) a Friedman test to assess the significance between baseline and follow-up, and 3) a Wilcoxon signed-rank test to compare the weighted mean CVR in each dose group in the baseline and follow-up. The mean CVR in each dose group was weighted by dividing the average CVR per group by the total amount of pixels in that group.

4 Results

4.1 Image Registration Pipeline

As described in the Methods, the pipeline is built for one ideal patient (APP003). After finishing the pipeline for the test patient, the pipeline is run for the other patients (13 in the baseline, five in the follow-up). The image registration pipeline performed well for most of the patients and most of the scans. The performance of the image registration is listed in Table 2. The pipeline did not have an optimal performance for four of the CT scans (APP005, APP009, APP0013, APP0014) and one T2FLAIRb scan (APP001). For these patients, adjustments had to be made to register the CT and T2FLAIRb accurately.

Table 2. Performance of the image registration pipeline. The baseline pipeline is run 13 times for 13 different patients and the follow-up pipeline is run five times for five follow-up patients.

Scan	Baseline	Follow-up
CT	9/13 (69%)	-
T1	-	5/5 (100%)
T2FLAIR	13/13 (100%)	4/5 (80%)
BOLD	13/13 (100%)	5/5 (100%)

In Figure 22, two examples are shown of the misregistration of a CT scan and the T2FLAIRb scan. All misregistrations of the CT registration would result in a completely flipped CT scan (Figure 22a). This problem could be resolved for two CT scans by lowering the value of the finesearch parameter to 2°. This reduction did not solve the misregistation of two other CT scans, and therefore, weighted volumes were generated and used during the registration. The weighted volume influences the cost function by setting some areas in the weighted volume to zero, these parts of the image will be ignored during the registration. For these two CT registrations a brain mask was generated in ITK-SNAP were the brain had a value of one and rest a value of zero. This volume helped with the registration algorithm to focus on the brain instead of other structures in the head. The misregistration of the T2FLAIRb scan (see Figure 22b), could be resolved by first registering T2FLAIRb to T1b and registering T2FLAIRb to T1 by combining the matrix from the T2FLAIR to T1b registration with the T1b to T1 registration. These adjustments were used to resolve the misregistered scans.

4.2 VOI-based Analysis

The average CVR is calculated for each segmentation around the tumour independent of GM and WM (see Table 3). These segmentations contain the brain without CSF and oedema. The oedema was extracted since it is unclear which type of tissue is in these areas. The average CVR increases slightly with an increasing distance from the tumour, however this increase is not significant ($p = 0.347$). The result of the WM and GM analysis is shown in Figure 23. The average CVR signal is significantly higher in the GM and lower in the WM ($p = 0.018$) . At an
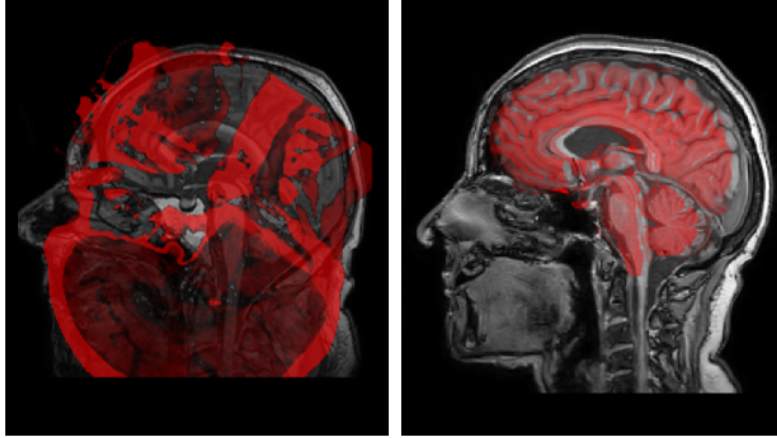
(a) CT   (b) T2FLAIRb

Fig. 22. Misregistrations of a CT (a) and a T2FLAIRb (b) scan. The reference image is show in grey values and the registered image is shown in red.

increasing distance from the tumour, the average CVR slightly increases. This increase is not significant in GM and WM since the p-values are 0.156 and 0.050, respectively. The VOI 2 to 7 are compared to VOI 1 and the furthest VOI (VOI 7) was significantly different from VOI 1 for GM ($p = 0.046$) and WM ($p = 0.039$). The average CVR increase in the other VOIs was not significant in comparison with VOI 1. In Appendix F, the CVR maps of all baseline patients are shown. The average CVR signal was similar between patients, except for patient APP015. This patient had an really high CVR in comparison to the other patients. The overall spread of CVR in the sections is quite high between patients which leads to large standard deviations.

Table 3. The average CVR in percentage BOLD signal change per mmHg CO_2 per VOI around the tumour.

Distance	Average CVR	SD
VOI 1 (2 pixels)	0.112	0.055
VOI 2 (4 pixels)	0.110	0.047
VOI 3 (6 pixels)	0.115	0.043
VOI 4 (8 pixels)	0.121	0.052
VOI 5 (10 pixels)	0.127	0.059
VOI 6 (12 pixels)	0.130	0.057
VOI 7 (14 pixels)	0.130	0.060
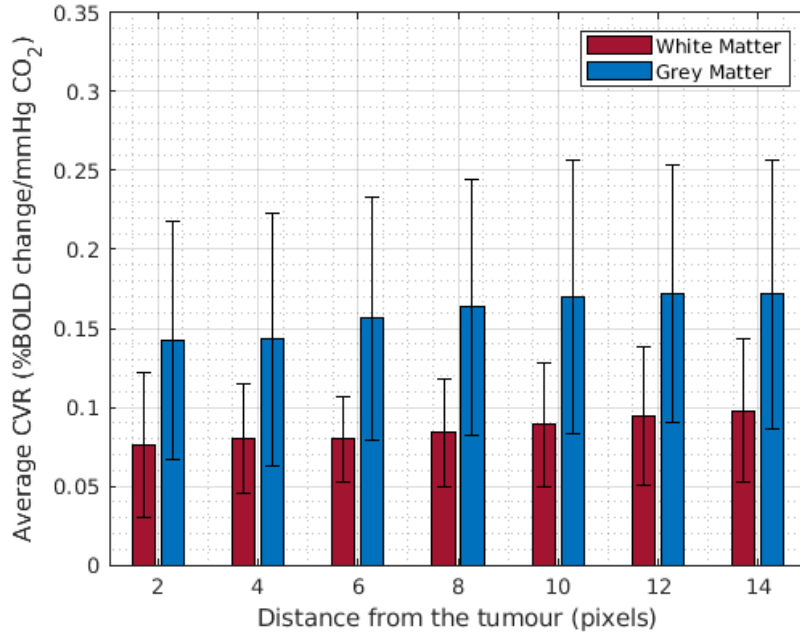
Fig. 23. The average CVR in GM and in WM in the different VOIs at increasing distance from the tumour. The error bars show the standard deviation of each bar.

4.3 Dose-based Analysis

In the dose-based analysis, the baseline CVR maps is compared to the follow-up CVR maps. The baseline and follow-up CVR maps of all patients in this analysis can be seen in Appendix F in Figure 32 and 33. The average CVR per dose group is calculated using the baseline and follow-up CVR maps of each patient, the results can be seen in Figure 24. The average CVR in the follow-up was higher for two patients (APP005 and APP007), equal for one patient (APP003), lower for two patients (APP001 and APP006).

In Figure 24, the follow-up scan of APP001 stands out the most. The follow-up scan is declining rapidly with an increasing received dose and the CVR becomes negative. This patient has surgical clips inside the brain that stayed there after surgery. These clips cause artefacts in the BOLD scan and led to this decrease of CVR values. In Figure 25, an example is shown of the BOLDb scan with the tumour and the CVRb map. This figure shows signal loss in the BOLDb scan at the right side and the bottom of the image. In the CVR map, this loss of BOLD signal resulted in an area with negative CVR. These artefacts are close to the tumour and inside the higher dose groups, which causes the CVR value in these groups to become negative. The artefacts in the BOLDb scan result in unrealistic CVR values in that area. Therefore, the decision is made to exclude APP001 from the the dose-based analysis.

The dose-based analysis is performed with APP003, APP005, APP006, and APP007. THe average CVR is calculated per dose group and in GM and WM. The results of this are shown in Figure 26. The average CVR is slightly lower in GM in follow-up scans in comparison to the baseline scans. In WM, the average CVR in the follow-up is almost equal for the <5 Gy, 5-8 Gy and 12-16 Gy group, higher for the 8-12 Gy group and lower in the $\geq$16 Gy group in comparison to the baseline. The difference in CVR in the follow-up and baseline was not

30
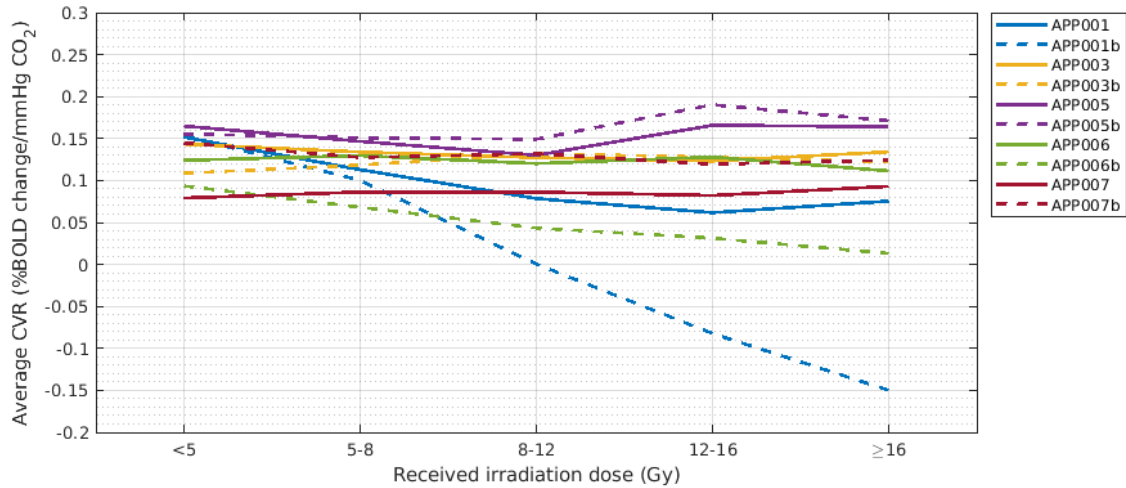
Fig. 24. The average CVR per patient per dose group in GM and WM combined.
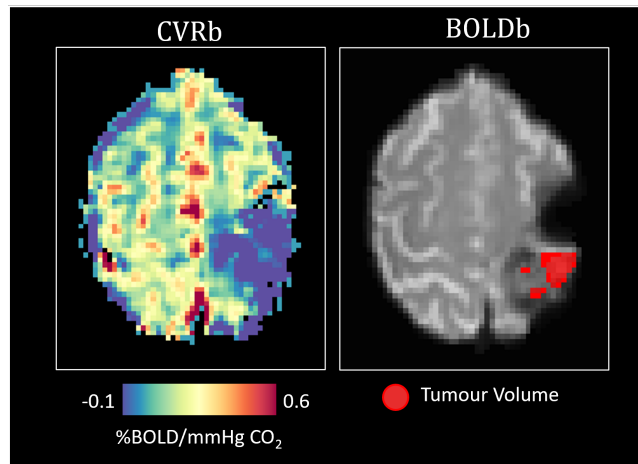
Fig. 25. The CVR map and the mean BOLD scan of APP001. This patient has surgical clips inside the brain. In the BOLDs scan loss of signal can be seen at the site of these clips in the right side and bottom of the image. This artefact resulted in negative CVR signal in that area.

significantly different in GM ($p = 0.627$), WM ($p = 0.185$), and combined ($p = 0.493$). The CVR in baseline and follow-up per dose group is also compared to each other and the difference between the follow-up and baseline was not significant. The p-values per dose group and per tissue type are listed in Table 4.

The follow-up and baseline values are compared regardless of the dose group. This was executed by calculating weighted follow-up and baseline CVR values. The CVR values are weighted by dividing the CVR value in the dose group by the number of pixels in that dose group. The follow-up and baseline did not differ significantly based on the weighted average CVR values per dose group. The p-values are 0.881, 0.263, and 0,627 for GM, WM, and the combined GM and WM, respectively.

An interaction plot is created to visualise a potential interaction between the received dose and time. In Figure 27, the average CVR values at baseline and at follow-up per dose group

31
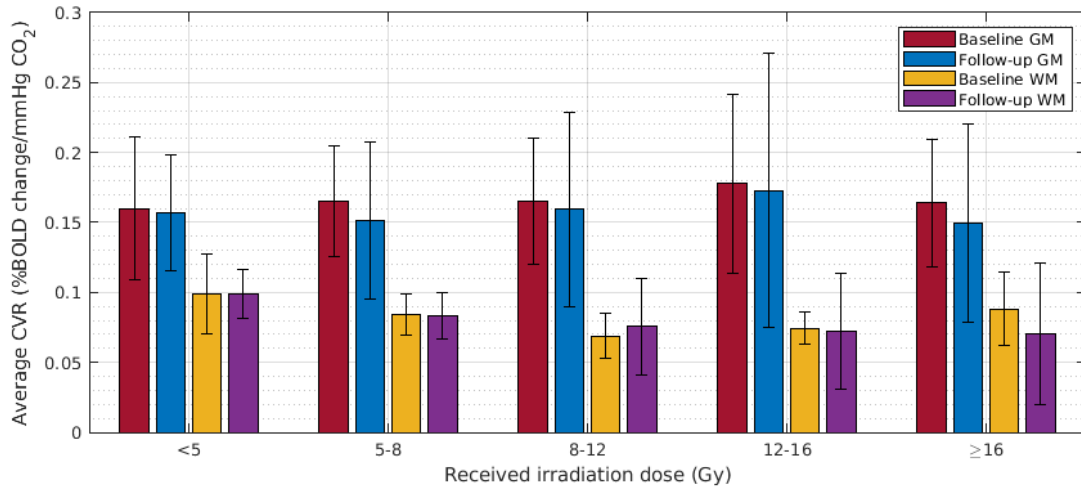
Fig. 26. The average CVR signal in GM and WM per dose group. The error bars depict the standard deviation per bar.

Table 4. p-values of the comparison between baseline and follow-up per dose group in GM and WM

Dose Groups	Grey Matter (p-value)	White Matter (p-value)
<5 Gy	0.715	0.715
5 - 8 Gy	0.715	0.715
8 - 12 Gy	1.000	0.715
12 - 16 Gy	0.715	0.715
≥16 Gy	1.000	0.465

are plotted for GM and WM. The response is higher in GM than in WM, which was expected. The CVR in GM in the dose groups 5-8 Gy and ≥16 Gy seems to decrease more than the <5 Gy group. The decrease in the <5 Gy, 8-12 Gy, and 12-16 Gy groups are decreasing slightly. In WM the CVR in the baseline and follow-up is similar in the <5 Gy, 5-8 Gy, and 12-16 Gy groups. The CVR signal decreases the most in the ≥16 Gy group and increases in the 8-12 Gy group.
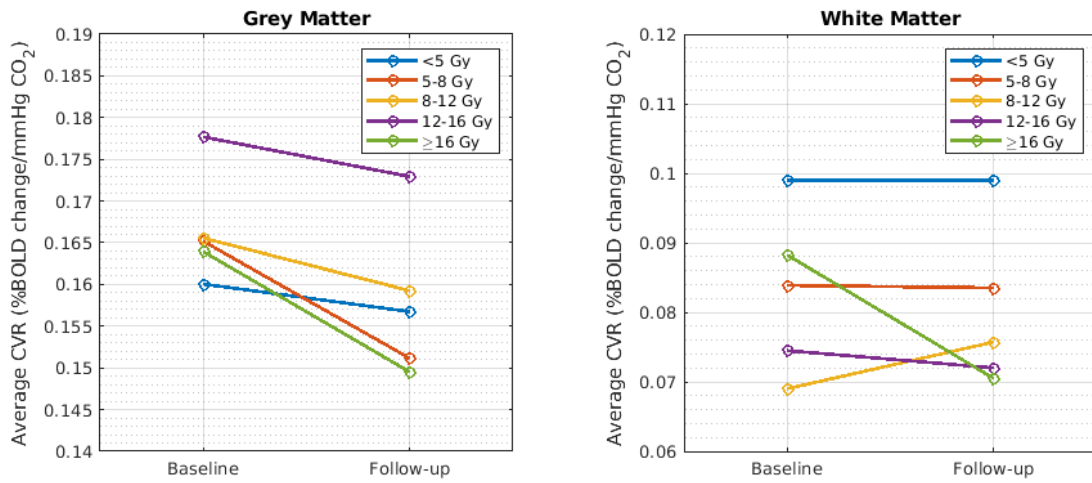
Fig. 27. Interaction plot with average CVR at baseline and follow-up per dose group in GM and WM.

5 Discussion

This thesis developed an image registration pipeline with close to optimal performance for most of the scans. The pipeline performed less well for the CT registration and the T2FLAIRb registration, where the pipeline registered the images in 69% and 80% of the cases, receptively. This image registration pipeline is ideal to be used by the researchers of the APRICOT study to improve efficacy by quickly registering all the scans of the baseline scans as well as the follow-up scans. In addition to the image registration pipeline, an analyses script is written that performs a VOI- and dose-based analysis.

The VOI-based analysis found that CVR was significantly increased at an increasing distance from the tumour in WM, where the p-value was precisely 0.05. The slight increase at an increasing distance from the tumour was not significant in GM for all VOIs. However, the first VOI (VOI 1) around the tumour was significantly lower than the latest VOI, 14 pixels from the tumour (VOI 7) in GM and WM. These results show that BM affects the CVR of the cerebrovasculature, which can be measured with the cerebrovascular stress test for patients with BM. The slight increase of CVR at an increasing distance from the tumour in the VOI-based analysis could be explained by the abnormal anatomy of vasculature around tumours. The blood vessels often are irregular structured, are more permeable, and have chaotic flow patterns [63,64]. This might lead to a poor function of vessels which will depict itself as a lower signal in a CVR map.

The dose-based analysis found a small decrease in follow-up CVR in comparison to baseline CVR in GM in patients with BM that received SRS. The difference was minuscule and not statistically significant. These results suggest a slight decrease in CVR, however, based on these results no conclusions can be yet be derived. The changes in CVR are related to the cognition of the patient [65]. Cognitive changes were observed by Chang et al. in 24% of the patients at four months after RT [66]. A review found little to no cognitive decline four months after SRS [67]. It might be the case that these patients do not have cognitive decline yet three months after RT, and therefore, no significant changes could be seen between baseline and follow-up CVR. The damage induced by radiation is cumulative, and the effects might develop in a later stage [68]. These things might have affected the results and can explain why no significant changes could be seen between baseline and follow-up CVR.

The results of this thesis are limited due to some limitations. All results were based on a small cohort of patients that underwent baseline (n=13) and follow-up (n=4), and therefore, the results are less reliable. A larger patient cohort is needed to further evaluate the outcomes. Moreover, especially the dose-based analysis is performed on a rather small data set. Thereby, two of the patients in this data (APP001 and APP005) set already received previous cranial RT. This could have already induced some damages in the vasculature and resulted in a lower baseline CVR measurement. The damage of radiation dose is cumulative and stochastic, therefore, the damage might occur in a later period.

The accuracy of the GM, WM, and CSF segmentations were also limited and specifically the GM segmentation. The GM segmentation sometimes included areas that did not contain any GM, this mostly occurred around the ventricles and the brain stem. These segmentations could be improved with other segmentation tools or a tool that gives probability segmentation maps [69]. Moreover, the GM segmentations also included oedema in the brains of the patients, which was extracted with a semi-automatic tool. Thereby, the false positives and false negatives

of the automatic segmentation had to be adjusted manually which can result in human errors and less accurate oedema segmentation. An alternative for the semi-automatic tool might be to use algorithms that are based on machine or deep learning that can accurately segment oedema and/or the tumour [70–72]. A more accurate WM, GM and CSF segmentation will lead to more reliable results.

The baseline analysis was executed with segmentations around the tumour (VOI-based), while generating the segmentation, the location of the tumour is not taken into account. For example, if the tumour is on the border of the right hemisphere, then the circular segmentations will also include the left hemisphere. This creates uncertainty in the data because the vessels in the unaffected hemisphere are not affected by the tumour in the affected hemisphere.This limitation could have been avoided by limiting the VOIs around the tumour to only expand in the affected hemisphere.

The registration is an additional limiting factor, where the interpolation methods introduced uncertainty in the data. The uncertainties due to interpolation methods are restricted by only interpolating an image once with a combined matrix instead of two or three times. Uncertainty due to registration is limited by visually inspecting all registrations to check the performance of the image registration pipeline.

The performed analysis is conducted with a categorical approach based on segmentations. This analysis can be broadened in future research by performing a voxel-wise analysis to look for potential correlations between CVR in patients with BM and the received dose. This study showed that CVR was not significantly reduced after RT. If these patients undergo cognitive decline after RT is uncertain at this moment in time. Therefore, additional research needs to be performed to relate CVR in BM patients with cognition. The APRICOT study performs this additional research by carrying out neurocogntive assessments of each patient at baseline and three months later at follow-up. The CVR maps together with neurocognitive assessments could potentially demonstrate a relationship between a reduced CVR and cognitive function in patients with BM that underwent RT.

Additional cognitive data could help to discover if the cognition of the patient changes three months after RT with SRS. A reduction of cognition can have a devastating effect on the patient's quality of life [73]. It would be optimal to determine the possible cognitive decline after RT to inform the patient of the possible cognitive decline. CVR provides information about the workings of the vasculature in the brain. If the CVR is already lower then the average, it could be possible to predict a further decline due to RT. Future prospect could be to test if baseline CVR is a feasible tool to predict the cognitive function of a patient after RT.

Patients with BM are already more likely to have or develop cognitive decline then other healthy persons [74]. Hence, cognitive decline is related to a lower CVR signal, additional research can be performed by comparing the CVR maps of healthy volunteers and patients with BM. This additional study create more understanding into CVR in patients with BM in comparison to healthy persons. In addition, it could potentially give more insight into the cognitive decline of patients with BM regardless of radiation-induced damage.

Although the performance of the pipeline is already ideal for the T2FLAIR, BOLD, BOLDb, and T1b registrations, the pipeline could be improved for the CT and T2FLAIRb scans. First, the reasons behind the misregistrations need to be investigated. The results of this could help to resolve the misregistrations of CT and T2FLAIRb and these solutions can be implemented into the image registration pipeline.

This thesis developed an accurate and high performance image registration pipeline that corrects for geometric distortion artefacts and registers a CT, T1-weighted, T2-weighted FLAIR, and BOLD scan. Subsequently, an analysis script is developed to evaluate the CVR in the cerebrovasculature of patients with BM. The results showed an increase of mean CVR at a distance from the tumour in GM and WM. These results indicate that BM influences the CVR of these patients. The CVR was slightly lower in GM after radiotherapy, but this difference was not significant. No major conclusions can be drawn based on these results. Further research needs to be conducted on a larger patient cohort to find out if CVR decreases after RT in patients with BM.

6   Conclusion

This thesis showed a slightly increasing CVR at a distance from the tumour, which could indicate that BM influences the CVR of the cerebrovasculature of these patients. Additional results showed a small difference between average baseline CVR and follow-up CVR in patients with brain metastases after stereotactic radiosurgery. The differences between the baseline CVR and follow-up CVR were too small to draw conclusions based on these results. Further research with a larger patient cohort needs to be conducted, to evaluate if CVR is reduced in patients with BM after stereotactic radiosurgery.

References

[1] R.A. Patchell. The management of brain metastases. *Cancer Treatment Reviews*, 29(6):533–540, 2003.

[2] J. Gállego Pérez-Larraya and J. Hildebrand. Brain metastases. *Handb Clin Neurol*, 121:1143–57, 2014.

[3] T.T. Lah, M. Novak, and B. Breznik. Brain malignancies: Glioblastoma and brain metastases. *Seminars in Cancer Biology*, 60:262–273, 2020.

[4] X. Lin and L.M. DeAngelis. https://doi.org/10.1200/jco.2015.60.9503Treatment of Brain Metastases. *J Clin Oncol*, 33(30):3475–84, 2015.

[5] V. Shah and P. Kochar. Brain Cancer: Implication to Disease, Therapeutic Strategies and Tumor Targeted Drug Delivery Approaches. *Recent Pat Anticancer Drug Discov*, 13(1):70–85, 2018.

[6] H. Aoyama, H. Shirato, M. Tago, K. Nakagawa, T. Toyoda, K. Hatano, M. Kenjyo, N. Oya, S. Hirota, H. Shioura, E. Kunieda, T. Inomata, K. Hayakawa, N. Katoh, and G. Kobashi. Stereotactic radiosurgery plus whole-brain radiation therapy vs stereotactic radiosurgery alone for treatment of brain metastases: a randomized controlled trial. *Jama*, 295(21):2483–91, 2006.

[7] M.T. Makale, C.R. McDonald, J.A. Hattangadi-Gluth, and S. Kesari. Mechanisms of radiotherapy-associated cognitive disability in patients with brain tumours. *Nat Rev Neurol*, 13(1):52–64, 2017.

[8] M. P. Mehta. The controversy surrounding the use of whole-brain radiotherapy in brain metastases patients. *Neuro Oncol*, 17(7):919–23, 2015.

[9] P. D. Brown, K. V. Ballman, J. H. Cerhan, S. K. Anderson, X. W. Carrero, A. C. Whitton, J. Greenspoon, I. F. Parney, N. N. I. Laack, J. B. Ashman, J. P. Bahary, C. G. Hadjipanayis, J. J. Urbanic, 2nd Barker, F. G., E. Farace, D. Khuntia, C. Giannini, J. C. Buckner, E. Galanis, and D. Roberge. Postoperative stereotactic radiosurgery compared with whole brain radiotherapy for resected metastatic brain disease (NCCTG N107C/CEC·3): a multicentre, randomised, controlled, phase 3 trial. *Lancet Oncol*, 18(8):1049–1060, 2017.

[10] M.H. Soike, R.T. Hughes, M. Farris, E.R. McTyre, C.K. Cramer, J.D. Bourland, and M.D. Chan. Does Stereotactic Radiosurgery Have a Role in the Management of Patients Presenting With 4 or More Brain Metastases? *Neurosurgery*, 84(3):558–566, 2019.

[11] C.G. Rusthoven, M. Yamamoto, D. Bernhardt, D.E. Smith, D. Gao, T. Serizawa, S. Yomo, H. Aiyama, Y. Higuchi, T. Shuto, A. Akabane, Y. Sato, A. Niranjan, A.M. Faramand, L.D. Lunsford, J. McInerney, L.C. Tuanquin, B.E. Zacharia, V. Chiang, C. Singh, J.B. Yu, S. Braunstein, D. Mathieu, C.J. Touchette, C.C. Lee, H.C. Yang, A.A. Aizer, D. N. Cagney, M.D. Chan, D. Kondziolka, K. Bernstein, J.S. Silverman, I.S. Grills, Z.A. Siddiqui, J. C. Yuan, J.P. Sheehan, D. Cordeiro, K. Nosaki, T. Seto, C.P. Deibert, V. Verma, S. Day,

L.M. Halasz, R.E. Warnick, D.M. Trifiletti, J.D. Palmer, A. Attia, B. Li, C.P. Cifarelli, P.D. Brown, J.A. Vargo, S.E. Combs, K.A. Kessel, S. Rieken, S. Patel, M. Guckenberger, N. Andratschke, B.D. Kavanagh, and T.P. Robin. Evaluation of First-line Radiosurgery vs Whole-Brain Radiotherapy for Small Cell Lung Cancer Brain Metastases: The FIRE-SCLC Cohort Study. *JAMA Oncol*, 6(7):1028–1037, 2020.

[12] P.D. Brown, K. Jaeckle, K.V. Ballman, E. Farace, J.H. Cerhan, S.K. Anderson, X.W. Carrero, F.G. Barker, R. Deming, S.H. Burri, C. Ménard, C. Chung, V.W. Stieber, B.E. Pollock, E. Galanis, J.C. Buckner, and A.L. Asher. Effect of Radiosurgery Alone vs Radiosurgery With Whole Brain Radiation Therapy on Cognitive Function in Patients With 1 to 3 Brain Metastases: A Randomized Clinical Trial. *Jama*, 316(4):401–409.

[13] S. Peters, C. Bexelius, V. Munk, and N. Leighl. The impact of brain metastasis on quality of life, resource utilization and survival in patients with non-small-cell lung cancer. *Cancer Treat Rev*, 45:139–62, 2016.

[14] J. Wong, A. Hird, A. Kirou-Mauro, J. Napolskikh, and E. Chow. Quality of life in brain metastases radiation trials: a literature review. *Curr Oncol*, 15(5):25–45, 2008.

[15] P.S. Sachdev, D. Blacker, D.G. Blazer, M. Ganguli, D.V. Jeste, J.S. Paulsen, and R.C. Petersen. Classifying neurocognitive disorders: the DSM-5 approach. *Nature Reviews Neurology*, 10(11):634–642, 2014.

[16] A.M. Sanford. Mild Cognitive Impairment. *Clin Geriatr Med*, 33(3):325–337, 2017.

[17] P.W. Sperduto, S.T. Chao, P.K. Sneed, X. Luo, J. Suh, D. Roberge, A. Bhatt, A.W. Jensen, P.D. Brown, H. Shih, J. Kirkpatrick, A. Schwer, L.E. Gaspar, J.B. Fiveash, V. Chiang, J. Knisely, C.M. Sperduto, and M. Mehta. Diagnosis-specific prognostic factors, indexes, and treatment outcomes for patients with newly diagnosed brain metastases: a multi-institutional analysis of 4,259 patients. *Int J Radiat Oncol Biol Phys*, 77(3):655–61, 2010.

[18] D. Greene-Schloesser, M.E. Robbins, A.M. Peiffer, E.G. Shaw, K.T. Wheeler, and M.D. Chan. Radiation-induced brain injury: A review. *Front Oncol*, 2:73, 2012.

[19] C. Wilke, D. Grosshans, J. Duman, P. Brown, and J. Li. Radiation-induced cognitive toxicity: pathophysiology and interventions to reduce toxicity in adults. *Neuro-Oncology*, 20(5):597–607, 2017.

[20] C. Soussain, D. Ricard, J.R. Fike, J.J. Mazeron, D. Psimaras, and J.Y. Delattre. CNS complications of radiotherapy and chemotherapy. *Lancet*, 374(9701):1639–51, 2009.

[21] Z. Yang, B. Bai, S.and Gu, S. Peng, W. Liao, and J. Liu. *Radiation-Induced Brain Injury After Radiotherapy for Brain Tumor*, book section 8. IntechOpen, 2015.

[22] Y.Q. Li, P. Chen, A. Haimovitz-Friedman, R.M. Reilly, and C.S. Wong. Endothelial apoptosis initiates acute blood-brain barrier disruption after ionizing radiation. *Cancer Res*, 63(18):5950–6, 2003.

[23] J.P. Warrington, N. Ashpole, A. Csiszar, Y.W. Lee, Z. Ungvari, and W.E. Sonntag. Whole brain radiation-induced vascular cognitive impairment: mechanisms and implications. *J Vasc Res*, 50(6):445–57, 2013.

[24] J.P. Warrington, A. Csiszar, M. Mitschelen, Y.W. Lee, and W.E. Sonntag. Whole brain radiation-induced impairments in learning and memory are time-sensitive and reversible by systemic hypoxia. *PLoS One*, 7(1):e30444, 2012.

[25] J.P. Warrington, A. Csiszar, D.A. Johnson, T.S. Herman, S. Ahmad, Y.W. Lee, and W.E. Sonntag. Cerebral microvascular rarefaction induced by whole brain radiation is reversible by systemic hypoxia in mice. *American journal of physiology. Heart and circulatory physiology*, 300(3):H736–H744, 2011.

[26] U.S. Yezhuvath, K. Lewis-Amezcua, R. Varghese, G. Xiao, and H. Lu. On the assessment of cerebrovascular reactivity using hypercapnia BOLD MRI. *NMR in biomedicine*, 22(7):779–786, 2009.

[27] T.J. Haight, R.N. Bryan, G. Erus, C. Davatzikos, D.R. Jacobs, M. D'Esposito, C.E. Lewis, and L.J. Launer. Vascular risk factors, cerebrovascular reactivity, and the default-mode brain network. *NeuroImage*, 115:7–16, 2015.

[28] D.J. Lythgoe, S.C.R. Williams, M. Cullinane, and H.S. Markus. Mapping of cerebrovascular reactivity using bold magnetic resonance imaging. *Magnetic Resonance Imaging*, 17(4):495–502, 1999.

[29] A. Ruitenberg, T. den Heijer, S.L. Bakker, J.C. van Swieten, P.J. Koudstaal, A. Hofman, and M.M. Breteler. Cerebral hypoperfusion and clinical onset of dementia: the Rotterdam Study. *Ann Neurol*, 57(6):789–94, 2005.

[30] D. Kim, T.M. Hughes, M.E. Lipford, S. Craft, L.D. Baker, S.N. Lockhart, C.T. Whitlow, S.E. Okonmah-Obazee, C.E. Hugenschmidt, M. Bobinski, and Y. Jung. Relationship Between Cerebrovascular Reactivity and Cognition Among People With Risk of Cognitive Decline. *Front Physiol*, 12:645342, 2021.

[31] E. N. Marieb and K. N. Hoehn. *The Central Nervous System*, pages 450–504. Pearson, 10 edition, 2016.

[32] M. MacGregor Sharp, S. Saito, A. Keable, M. Gatherer, R. Aldea, N. Agarwal, J. Simpson, S. Wharton, R. Weller, and R. O. Carare. Demonstrating a reduced capacity for removal of fluid from cerebral white matter and hypoxia in areas of white matter hyperintensity associated with age and dementia. *Acta Neuropathologica Communications*, 8, 2020.

[33] J Hornak. *The basics of MRI*. 2010.

[34] R. B. Buxton. *Nuclear magnetic resonance*, pages 67–84. Cambridge University Press, Cambridge, 2 edition, 2009.

[35] S. Currie, N. Hoggard, I. J. Craven, M. Hadjivassiliou, and I. D. Wilkinson. Understanding MRI: basic MR physics for physicians. *Postgrad Med J*, 89(1050):209–23, 2013.

[36] R. W. Brown, Y. N. Cheng, E. M. Haacke, M. R. Thompson, and R. Venkatesan. *Magnetic Field Inhomogeneity Effects and T2* Dephasing*, pages 569–617. 2014.

[37] P.W. Stroman. *Essentials of Functional MRI (1st ed.)*. CRC Press., 2011.

[38] A. D. Elster and J. H. Burdette. *Questions and Answers in MRI, 2nd ed*, pages 72–101. 2001.

[39] D. Moratal, A. Vallés-Luch, L. Martí-Bonmatí, and M. Brummer. k-Space tutorial: an MRI educational tool for a better understanding of k-space. *Biomed Imaging Interv J*, 4(1):e15, 2008.

[40] 3rd Mugler, J. P. and J. R. Brookeman. Rapid three-dimensional T1-weighted MR imaging with the MP-RAGE sequence. *J Magn Reson Imaging*, 1(5):561–7, 1991.

[41] J. S. Ross. Newer sequences for spinal MR imaging: smorgasbord or succotash of acronyms? *AJNR. American journal of neuroradiology*, 20(3):361–373, 1999.

[42] R. Bitar, G. Leung, R. Perng, S. Tadros, A. R. Moody, J. Sarrazin, C. McGregor, M. Christakis, S. Symons, A. Nelson, and T. P. Roberts. MR pulse sequences: what every radiologist wants to know but is afraid to ask. *Radiographics*, 26(2):513–37, 2006.

[43] R.B. Buxton. The physics of functional magnetic resonance imaging (fMRI). *Rep Prog Phys*, 76(9):096601, 2013.

[44] Q. Qin, K. Grgac, and P.C. van Zijl. Determination of whole-brain oxygen extraction fractions by fast measurement of blood T2 in the jugular vein. *Magn Reson Med*, 65(2):471–9, 2011.

[45] Marco Giannelli, Stefano Diciotti, Carlo Tessa, and Mario Mascalchi. Characterization of Nyquist ghost in EPI-fMRI acquisition sequences implemented on two clinical 1.5 T MR scanner systems: Effect of readout bandwidth and echo spacing. *Journal of applied clinical medical physics / American College of Medical Physics*, 11:3237, 2010.

[46] M. Poustchi-Amin, S. A. Mirowitz, J. J. Brown, R. C. McKinstry, and T. Li. Principles and applications of echo-planar imaging: a review for the general radiologist. *Radiographics*, 21(3):767–79, 2001.

[47] A. Battisti-Charbonney, J. Fisher, and J. Duffin. The cerebrovascular response to carbon dioxide in humans. *J Physiol*, 589(Pt 12):3039–48, 2011.

[48] A. A. Bhogal. *Mapping Brain Physiology Using Gas Challenges*. PhD thesis, University Medical Center Utrecht, 2016.

[49] S. Klein, M. Staring, K. Murphy, M. A. Viergever, and J. P. Pluim. elastix: a toolbox for intensity-based medical image registration. *IEEE Trans Med Imaging*, 29(1):196–205, 2010.

[50] J. West, J. M. Fitzpatrick, M. Y. Wang, B. M. Dawant, Jr. Maurer, C. R., R. M. Kessler, R. J. Maciunas, C. Barillot, D. Lemoine, A. Collignon, F. Maes, P. Suetens, D. Vandermeulen, P. A. van den Elsen, S. Napel, T. S. Sumanaweera, B. Harkness, P. F. Hemler, D. L. Hill, D. J. Hawkes, C. Studholme, J. B. Maintz, M. A. Viergever, G. Malandain, R. P. Woods, and et al. Comparison and evaluation of retrospective intermodality brain image registration techniques. *J Comput Assist Tomogr*, 21(4):554–66, 1997.

[51] M. Jenkinson and S. Smith. A global optimisation method for robust affine registration of brain images. *Med Image Anal*, 5(2):143–56, 2001.

[52] A. Roche, G. Malandain, X. Pennec, and N. Ayache. *The Correlation Ratio as a New Similarity Measure for Multimodal Image Registration*, volume 1496. 1998.

[53] Analysis Group FMRIB Oxford UK. Registration: Cost Functions, Interpolation and Masks, 2020. Accessed: 30-07-2021.

[54] D. N. Greve and B. Fischl. Accurate and robust brain image alignment using boundary-based registration. *Neuroimage*, 48(1):63–72, 2009.

[55] J. Modersitzki. *Fair: Flexible Algorithms for Image Registration*. Society for Industrial and Applied Mathematics, 2009.

[56] Thornhill Medical. *RespirAct RA-MR Operator's Manual*. 2017.

[57] M. Jenkinson, P. Bannister, M. Brady, and S. Smith. Improved optimization for the robust and accurate linear registration and motion correction of brain images. *Neuroimage*, 17(2):825–41, 2002.

[58] S.M. Smith, M. Jenkinson, M.W. Woolrich, C.F. Beckmann, T.E. Behrens, H. Johansen-Berg, P.R. Bannister, M. De Luca, I. Drobnjak, D.E. Flitney, R.K. Niazy, J. Saunders, J. Vickers, Y. Zhang, N. De Stefano, J.M. Brady, and P.M. Matthews. Advances in functional and structural MR image analysis and implementation as FSL. *Neuroimage*, 23 Suppl 1:S208–19, 2004.

[59] J.L. Andersson, S. Skare, and J. Ashburner. How to correct susceptibility distortions in spin-echo echo-planar images: application to diffusion tensor imaging. *Neuroimage*, 20(2):870–88, 2003.

[60] Y. Zhang, M. Brady, and S. Smith. Segmentation of brain MR images through a hidden Markov random field model and the expectation-maximization algorithm. *IEEE Trans Med Imaging*, 20(1):45–57, 2001.

[61] A. A. Bhogal. seeVR a toolbox for analyzing cerebro-vascular reactivity data. `https://www.seevr.nl/`, 2021.

[62] P. Schmidt and L. Wink. LST: A lesion segmentation tool for SPM. `https://www.applied-statistics.de/LST_documentation.pdf`, 2019.

[63] D. W. Siemann. The unique characteristics of tumor vasculature and preclinical evidence for its selective disruption by Tumor-Vascular Disrupting Agents. *Cancer treatment reviews*, 37(1):63–74, 2011.

[64] J. A. Nagy, S. H. Chang, A. M. Dvorak, and H. F. Dvorak. Why are tumour blood vessels abnormal and why is it important to know? *Br J Cancer*, 100(6):865–9, 2009.

[65] Rebecca J. Williams, M. Ethan MacDonald, Erin L. Mazerolle, and G. Bruce Pike. The Relationship Between Cognition and Cerebrovascular Reactivity: Implications for Task-Based fMRI. *Frontiers in Physics*, 9(157), 2021.

[66] E.L. Chang, J.S. Wefel, K.R. Hess, P.K. Allen, F.F. Lang, D.G. Kornguth, R.B. Arbuckle, J.M. Swint, A.S. Shiu, M.H. Maor, and C.A. Meyers. Neurocognition in patients with brain metastases treated with radiosurgery or radiosurgery plus whole-brain irradiation: a randomised controlled trial. *Lancet Oncol*, 10(11):1037–44, 2009.

[67] W. C. M. Schimmel, K. Gehring, D. B. P. Eekers, P. E. J. Hanssens, and M. M. Sitskoorn. Cognitive effects of stereotactic radiosurgery in adult patients with brain metastases: A systematic review. *Adv Radiat Oncol*, 3(4):568–581, 2018.

[68] Y. Puckett and T. M. Nappe. *Ionizing Radiation*. StatPearls Publishing Copyright © 2021, StatPearls Publishing LLC., Treasure Island (FL), 2021.

[69] Eileanoir B. Johnson, Sarah Gregory, Hans J. Johnson, Alexandra Durr, Blair R. Leavitt, Raymund A. Roos, Geraint Rees, Sarah J. Tabrizi, and Rachael I. Scahill. Recommendations for the Use of Automated Gray Matter Segmentation Tools: Evidence from Huntington's Disease. *Frontiers in neurology*, 8:519–519, 2017.

[70] N. Ironside, C. J. Chen, S. Mutasa, J. L. Sim, D. Ding, S. Marfatiah, D. Roh, S. Mukherjee, K. C. Johnston, A. M. Southerland, S. A. Mayer, A. Lignelli, and E. S. Connolly. Fully Automated Segmentation Algorithm for Perihematomal Edema Volumetry After Spontaneous Intracerebral Hemorrhage. *Stroke*, 51(3):815–823, 2020.

[71] A. Demirhan, M. Toru, and I. Guler. Segmentation of tumor and edema along with healthy tissues of brain using wavelets and neural networks. *IEEE J Biomed Health Inform*, 19(4):1451–8, 2015.

[72] A.M. Koning. Automated Cerebral Edema Segmentation in Patients with Intracerebral Hemorrhage Using 2D and 3D Deep Learning, 2018.

[73] J. Li, S. M. Bentzen, J. Li, M. Renschler, and M. P. Mehta. Relationship between neurocognitive function and quality of life after whole-brain radiotherapy in patients with brain metastasis. *Int J Radiat Oncol Biol Phys*, 71(1):64–70, 2008.

[74] A. Gerstenecker, L. B. Nabors, K. Meneses, J. B. Fiveash, D. C. Marson, G. Cutter, R. C. Martin, C. A. Meyers, and K. L. Triebel. Cognition in patients with newly diagnosed brain metastasis: profiles and implications. *J Neurooncol*, 120(1):179–85, 2014.

[75] N. Hegemann, M. Guckenberger, C. Belka, U. Ganswindt, F. Manapov, and M. Li. Hypofractionated radiotherapy for prostate cancer. *Radiation Oncology*, 9(1):275, 2014.

[76] D.H. Brand and J.R. Yarnold. The Linear-Quadratic Model and Implications for Fractionation. *Clin Oncol (R Coll Radiol)*, 31(10):673–677, 2019.

[77] A. Santacroce, M.A. Kamp, W. Budach, and D. Hänggi. Radiobiology of radiosurgery for the central nervous system. *Biomed Res Int*, 2013:362761, 2013.

[78] N.G. Burnet, S.J. Thomas, K.E. Burton, and S.J. Jefferies. Defining the tumour and target volumes for radiotherapy. *Cancer Imaging*, 4(2):153–61, 2004.

[79] M. Jenkinson, P. Bannister, M. Brady, and S. Smith. Improved optimization for the robust and accurate linear registration and motion correction of brain images. *Neuroimage*, 17(2):825–41, 2002.

[80] S. M. Smith. Fast robust automated brain extraction. *Hum Brain Mapp*, 17(3):143–55, 2002.

Appendix A   Supplementary Patient Information

Table 5. Characteristics of the included patients. The brain metastases column refers to the number of BM patients received treatment for. All patients received SRS, which means that the treatment dose is given in one fraction. Some patients already received previous cranial RT in the form of SRS or primary radiation treatment with three fractions. Only the first five included patients underwent the follow-up scan.

Patients	Brain metastasis	Treatment Dose	Previous RT	Follow-up
APP001	4	18 Gy	2x	yes
APP003	7	24 Gy	-	yes
APP005	1	21 Gy	4x	yes
APP006	2	21 Gy	-	yes
APP007	11	24 Gy	-	yes
APP008	2	18 Gy	-	-
APP009	12	24 Gy	-	-
APP010	5	24 Gy	-	-
APP011	8	24 Gy	-	-
APP012	9	24 Gy	-	-
APP013	2	24 Gy	-	-
APP014	4	24 Gy	1x	-
APP015	2	18 Gy	2x	-

Appendix B CT-data pre-processing

The CT data was obtained from the clinical radiotherapy servers of the UMC Utrecht in the Netherlands. The dose distributions of the patients are recalculated to obtain the same equivalent dose per 2 Gy fractions (EQD_2). The Linear Quadratic (LQ) Model (Equation 5) is used to calculate the the EQD_2 for each patient.

$$EQD_2 = n \cdot d \cdot \frac{(d + \frac{\alpha}{\beta})}{(2 + \frac{\alpha}{\beta})} \tag{5}$$

where d is the dose per fraction, n is the number of fractions, and α/β is a ratio. The LQ model describes a relationship between cell survival and delivered dose. The α/β ratio is a measure of the sensitivity to fractionation of the cells, where a high ratio is less sensitive, and a low ratio is more sensitive to the effect of fractionation of RT [75, 76]. Tumours in the central nervous system, such as BM are classified as late responding tissue and typically have a α/β ratio of 2 [77].

On a CT scan, the BM and the organs at risk are delineated by the clinician and are referred to as planning VOIs. The tumour tissue is delineated as a gross tumour volume (GTV), clinical target volume (CTV), and planning target volume (PTV). The GTV describes the visible tumour. The CTV contains the GTV and a margin for the microscopic extent of the tumour. The last volume, the PTV, contains the GTV and CTV and allows for uncertainties in the treatment delivery. [78]

The brain tumours in the UMC Utrecht are mostly delineated with a GTV and a PTV. A mask of the baseline tumour were created for all the included patients. This mask is made by giving the background and the brain a value of 0, PTV a value of 3, and GTV a value of 1.

After obtaining the CT-scan, tumour mask and dose distribution of a patient, the data is converted from DICOM to NIfTI format with the *dcm2niix* convertor. NIfTI format stands for Neuroimaging Informatics Technology Initiative and is a globally used data format for neuroimaging. Subsequently, the CT data is transferred to the research servers of the UMC Utrecht.

Appendix C   MRI Scanning Parameters

Table 6. MRI parameters of the MRI scanning protocol

MRI-sequence	Parameters
3D TFE T1-weighted	TR 8 ms, TE 3.25 ms, flip angle 10°, slices 180, slice thickness 1 mm, matrix size is 240x240
3D TIR T2-weighted FLAIR	TR 4800 ms, TE 340 ms, flip angle 90°, slices 182, slice thickness 1.123 mm, matrix size is 256x256
BOLD EPI	TR 1050 ms, TE 30 ms, flip angle 65°, slices 51, slice thickness 2.5 mm, matrix size is 96x96

Appendix D   Pipeline Development

This appendix will explain the development of the analysis pipeline. This image analysis pipeline was built to bring all acquired scans in spatial correspondence to be able to perform a data analysis of the baseline CVR map and the follow-up CVR maps. This pipeline accomplishes this by removing certain artefacts from the scans and registering the scans into one corresponding space. The pipeline was built first for one ideal patient (APP003). This patient had scanning data with no artefacts and performed the breathing challenges sufficiently. The image analysis pipeline needs to register the following data sets to the baseline T1 scan: baseline CT scan with dose distribution and tumour mask, baseline BOLD scan, baseline T2FLAIR scan, follow-up T1 scan, follow-up T2FLAIR, follow-up BOLD.

The pipeline is built on the research servers of the UMC Utrecht and consists of two separate bash scripts, one script for the baseline and one script for the follow-up data. The bash scripts work with scans in NIfTI format files, which stands for Neuroimaging Informatics Technology Initiative and is a globally used data format for neuroimaging. The data is processed and registered using the FSL analysis toolbox for brain imaging data.

In Section 2.4, it was mentioned that for every registration, the cost function, the DOF, and interpolation method needs to be selected. The cost functions were selected by registering the moving images to the reference images with all applicable cost functions. The registrations were performed using six or 12 DOF to select the most optimal number of DOF. The interpolation method was chosen per registration based on the type of data (scan or mask/segmentation) and the function of that type of data in the data analysis. The results of all registrations were visually analysed using ITK-SNAP, and the best option was selected for the pipeline registration.

Prior to the registration of the anatomical scans (T1, T1b, T2FLAIR, and T2FLAIRb), the brain is extracted using FSL BET (Brain Extraction Tool). The extracted brains are registered to each other, which helps the registration tool to focus on registering the brain perfectly. Afterwards, the resulting transformation matrix is used to resample the whole scan to T1 space.

D.1   Baseline Registration Pipeline

The baseline pipeline needed to register the CT scan with dose distribution and tumour mask, baseline BOLD scan, and baseline T2FLAIR scan to the baseline T1 scan. The following sections will describe the process of these three registrations.

D.1.1   CT Registration

The registration of the CT to T1 scan, is executed using FSL FLIRT (FMRIB's Linear Image Registration Tool). This registration requires an inter-modal cost function and the available inter-modal cost functions for FLIRT are correlation ratio (corratio), mutual information (mutualinfo), and normalised mutual information (normcorr).

At first, all tried options did not result in an optimal registration of CT to T1 space, because the registration tool had flipped the CT scan in an inaccurate position. The amount that the moving image can rotate during the registration can be defined in FLIRT with the

option finesearch (input needs to be in degrees). The input for finesearch is chosen by visual inspection of the CT and T1 data. The orientation of the CT and T1 scans was quite similar, however, the CT scan was slightly tiled upwards in comparison to the T1 scan. Therefore, the finesearch parameter was set at a small angle (5°), and the registration was run again for all three cost functions. The results were visually analysed by comparing the registered CT scans to each other and to the T1 scan. The histograms and images of the three registered CT scans were comparable. In Table 7, the results of these three registrations are described. The cost function normmi, gave the best result and was selected as the cost function for the CT to T1 registration.

After visual inspection, the CT scan seemed to be nicely registered in some areas but slightly off in other areas. The registration was run again with an affine registration instead of a rigid registration, which resulted in a nicely registered CT scan. Therefore, the decision was made to implement an affine registration for the CT scans into the baseline bash script.

The resolution or look of the registered CT scan was not of concern because the CT will not be used in the CVR analysis. Hence, trilinear interpolation was used for the CT to T1 registration. The transformation matrix of this registration was most important since it is needed to register the dose distribution and tumour mask to T1 space. The values in the tumour mask should stay integers, and therefore, NN interpolation is selected to register the tumour mask to T1 space. The dose distribution is also registered with NN interpolation to ensure to keep the original dose values. Spline was not selected, since it can create values that are higher or lower than the maximum or minimum of the original image. This would make the dose distribution less reliable.

Table 7. The results of the registration of the CT scan to the T1 scan while making use of different cost functions

Cost Function	Description
corratio	The head of the patient was tilted downward in the CT scan in comparison to the T1 scan
mutualinfo	CT scan and T1 scan aligned quite well, however, there was a slight tilt backwards in the CT scan
normmi	The CT scan and T1 scan aligned well

D.1.2   T2FLAIR Registration

First, the brains of the T2FLAIR and T1 are coregistered, and afterwards, the tranformation matrix is used to register the entire T2FLAIR to T1 space. There are intensity differences between the T1 and T2FLAIR, and therefore, the cost functions leastsq and normcorr are not sufficient. The inter-modal cost functions, corratio, mutualinfo, and normmi, need to be used. All three optioned registered the T2FLAIR scan sufficiently, and no differences could be observed between the scans and their histograms (see Table 8). The cost function normmi was arbitrarily selected as the cost function for this registration.

The registration of T2FLAIR with normmi was repeated with affine and rigid registration. Affine registration scaled down the T2FLAIR brain in comparison to the T1 brain. In addition, the two scans were acquired after each other, and therefore, the movement between both scans is minimal. Rigid registration in combination with trilinear interpolation is selected for this part of the image registration pipeline. NN interpolation resulted in 'blocky' edges and created line artefacts in the image. In the T2FLAIR of all patients, abnormalities are visible such as the BM and oedema, and these abnormalities could be spread out with spline interpolation.

Table 8. The results of the registration of the T2FLAIR scan to the T1 scan while making use of the the cost functions: corratio, mutualinfo, and normmi.

Cost Function	Description
corratio	The T2FLAIR looks well registered to the T1
mutualinfo	This cost function also registered the T2FLAIR to the T1 quite well
normmi	No difference could be obeserved between mutualinfo and normmi. Normmi registered the T2FLAIR well with the T1.

D.1.3 BOLD registration

The first tries of the BOLD to T1 coregistration did not register the BOLD scan because borders of the brain in the BOLD scan could not line up the T1. This problem was caused by geometric distortions that were induced in the phase encoding direction (see Section 2.2.3). The section below will describe how this distortion is corrected in the analysis pipeline. Subsequently, the following sections will describe the baseline registration of the corrected BOLD to the baseline T1 scan.

Removing geometric distortions in BOLD scan
Inhomogeneities in the main magnetic field cause geometric distortions in the BOLD image and can lead to difficulties when registering the BOLD to the T1 scan. FSL has a function called topup that is able to correct for these distortions by using two data sets with reversed phase encoding directions. The phase encoding of the 17-minute long BOLD scan is in the anterior-posterior (AP) direction. After this long scan, a short acquisition is performed with the phase encoding in the reversed posterior-anterior (PA) direction. The topup function will use both scans to calculate a susceptibility-induced off-resonance field and create one corrected scan [58, 59].

Before topup is applied, the BOLD scan is motion-corrected. The scan is considerably long and the patient is undergoing breathing challenges, which makes it more likely for the patient to move during the scan. To perform the motion correction, the FLS function MCFLIRT is used [79]. Afterwards, the first time volume of the long BOLD scan (B_dn) and short acquisition (B_up) is taken and merged into one file (B_all) with the two time points after each other. Topup uses B_all to calculate a volume of field correction coefficients that the function will give as output. This volume of field correction coefficients is applied to the motion-corrected BOLD

scan with the FSL applytopup function. In Figure 28, an example of the distortions and the corrected result can be seen.
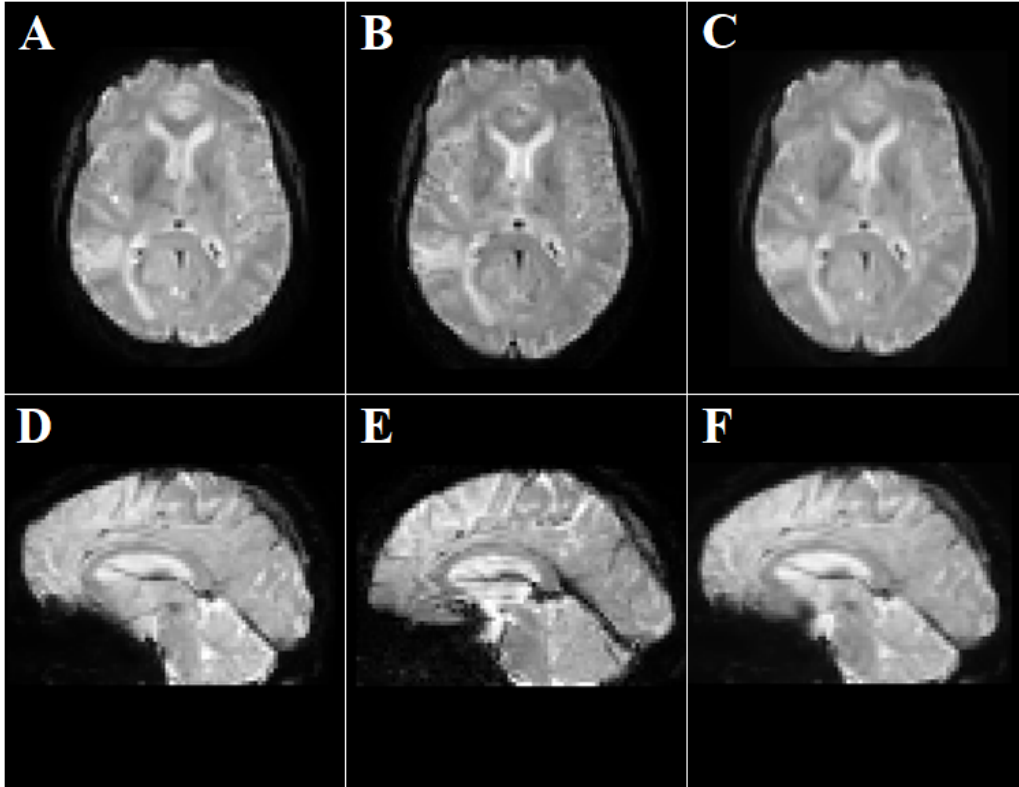
Fig. 28. This figure shows the distortions that were seen in the BOLD scans. The top row gives an axial view of the brain, and the bottom row shows the brain in a sagittal view. Image **A** and **D**, are taken with phase encoding direction AP. The distortions can be seen at the front of the brain, where there are 'dips' visible. The front of the brain looks like it has been pressed inwards (**A**). Image **B** and **E**, are taken in the reverse phase encoding direction, PA. This results in a brain that looks 'stretched'. The last column shows the results after topup is applied (image **C** and **F**).

BOLD Registration

The registration of the baseline BOLD scan is achieved with the FSL function epi_reg. This function is a specialised FLIRT function specially made for EPI images and uses the BBR cost function (see Section 2.4.1). Epi_reg needs the input of a structural scan with clear white matter boundaries and an EPI scan that contains intensity differences between white and grey matter. The function needs a WM segmentation as input or will calculate a WM boundary.

Before running epi_reg, a WM segmentation and a brain extraction of the T1 scan is created using FAST (FMRIB's Automated Segmentation Tool) and BET (Brain Extraction Tool), respectively. FAST generates segmentations of the GM, WM and CSF [60] and BET extracts the brain from the 3D scan and generates a mask of the brain [80]. In the epi_reg function, the interpolation method and DOF cannot be specified. However, the field correction of the top

up and the phase encoding direction can be specified to assist the function to make a sufficient registration. Epi_reg uses rigid registration and spline as the interpolation method.

D.2   Follow-up Registration Pipeline

The follow-up registration pipeline needs to register the T1b, T2FLAIRb, and BOLDb to the baseline T1 scan. In the sections below, the development of this part of the pipeline is discussed.

D.2.1   T1b Registration

This is the only registration were an intra-modal cost function can be used. Therefore, two registrations were performed using leastsq and normcorr. In Table 9, the results of the registration with both intra-modal cost functions is described. There was no visible difference between both cost functions and histograms looked similar. The cost function normcorr is selected because it performs better with intensity differences between the scans. There might be some intensity differences between the T1 and T1b scans of the other included patients, and normcorr is more reliable in generating good registrations for scans with these differences.

The registration is repeated with an affine and rigid registration. The affine method elongated the brain in the vertical direction (front to back) and shrunk the brain in the horizontal direction (left to right). The rigid method made a better registration and was chosen for this part of the pipeline. As already mentioned, abnormalities in the brain can be spread out with spline interpolation, and NN interpolation can make the image look 'blocky' or create line artefacts in the image. Trilinear interpolation was, therefore, selected as the interpolation method.

Table 9. The results of the registration of the T1b scan to the T1 scan while making use of the two intra-modal cost functions: leastsq and normcorr

Cost Function	Description
leastsq	After visual inspection the T1b looks well registered to the T1.
normcor	This cost funtion also registered the T1b to T1 well and no differences could be seen with the registraiton with leastsq.

D.2.2   T2FLAIRb Registration

This registration has to be executed with one of the three inter-modal cost functions. The results of the registrations are described in Table 10. No difference could be seen between corratio and normmi. The normmi cost function is selected again, since normmi is already used for all other registrations.

The registration was repeated with affine and rigid registration. Affine registration caused the brain to deform, and therefore, rigid is chosen for this registration. Trilinear interpolation is selected for this registration using the same reasoning that was given in the T1b registration.

Table 10. The results of the registration of the T2FLAIRb scan to the T1 scan while making use of the the cost functions: corratio, mutualinfo, and normmi.

Cost Function	Description
corratio	This cost function registered the T2FLAIRb well with the T1.
mutualinfo	This function slightly rotated the T2FLAIRb brain in the coronal view of the brain.
normmi	The T2FLAIRb was well registered to the T1 and there was no difference visable between the registered T2FLAIRb with corratio.

D.2.3 BOLDb Registration

Before BOLDb is registered to T1, the scan is corrected for motion and geometric distortions. This is performed with the same process that is described in the baseline BOLD registration.

For this registration, there were two possible options. The first option registered BOLDb directly to T1 with epi_reg. The second option has three different steps. First, BOLDb is registered to T1b with epi_reg. Secondly, the resulting matrix is multiplied with the transformation matrix of the T1b to T1 registration. Finally, the combined matrix will directly register BOLDb to T1 with normii and spline as the interpolation method. The cost function normmi is selected because it performed best most of the other registrations and spline interpolation was selected because this was also performed on the baseline BOLD with epi_reg.

For the test patient, both options gave a good registration. However, option one could result in problems when there are more anatomical differences between the follow-up and the baseline scans. Most patients have an increase or reduction in oedema at follow-up. For this reason, option two seemed more reliable and was selected for the BOLDb registration. The resulting matrix of this registration can be used to register BOLDb derivatives such as the CVR map to the baseline T1 space.

Appendix E Grey Matter Segmentation

As described in Section 3.6.1, most of the patients have oedema in the brain that leads to errors in the GM segmentation of the T1 scan that are generated with FSL FAST. These GM segmentations are corrected by extracting an oedema mask that is created with a semi-automatic segmentation tool using LST and ITK-SNAP. LST is a toolbox for SPM that can segment hyperintense legions using T2FLAIR scans. This tool was originally developed for the segmentation of multiple sclerosis lesions and has been shown to successfully segment other types of brain lesions such as legions from Alzheimer's disease [62]. LST has two tools the lesion growth algorithm (LGA) and the lesion prediction algorithm (LPA). LGA uses T2FLAIR and T1 scans to segment the lesions.

For each patient, the T1 and T2FLAIR scan are loaded into the LST program and an initial threshold (κ) is specified. The best κ for the data is obtained by visually inspecting the results. After running the program with several κs from 0.1 to 0.3, the κ that gave the best oedema segmentation was a κ of 0.14. The LST algorithm returns a mask with the segmented lesions. An example of a segmentation that was made by this tool can be seen in Figure 29. The false positives that were generated with this tool were manually erased and the places that the tool missed were manually adjusted in ITK-SNAP. The resulting oedema masks were extracted from the GM segmentation in the data analysis MATLAB script. The scripts can be found in Appendix H.

(a)   (b)
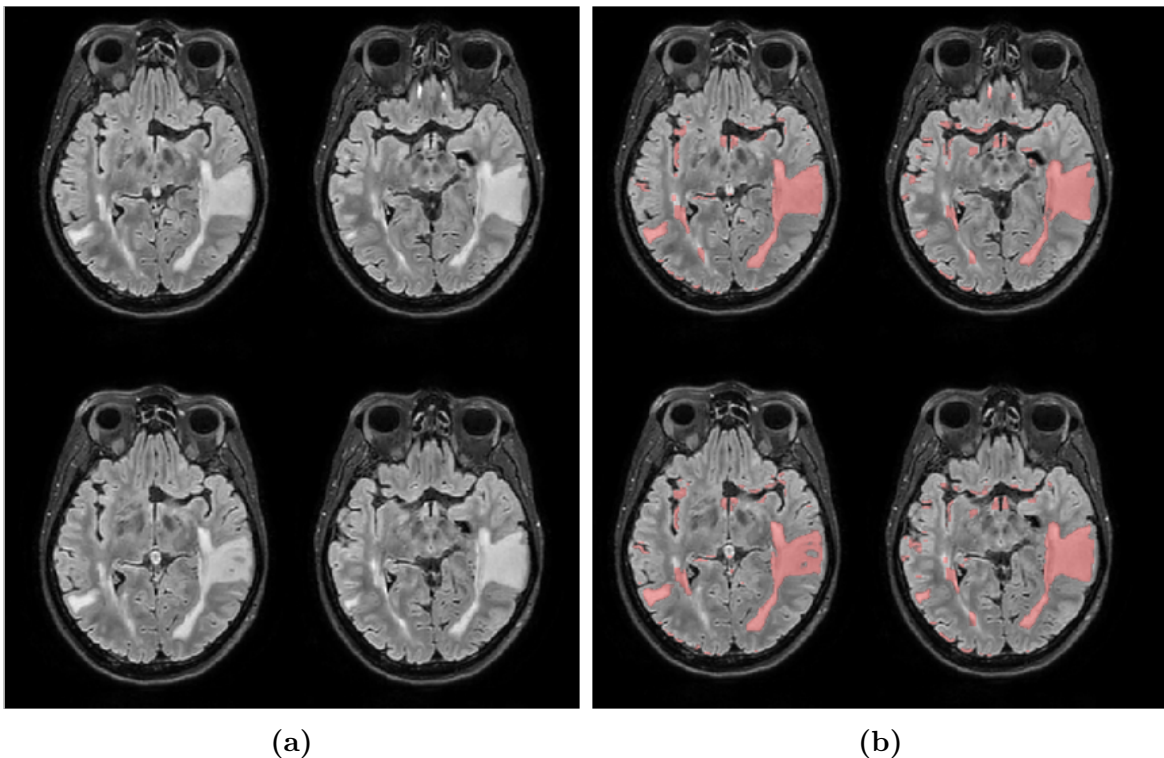
Fig. 29. Illustration of the automatic segmentations generated by the LST tool LGA. a) Shows the T2FLAIR of APP003 and b) Shows the segmentations in pink in the same T2FLAIR scan. The oedema is mostly segmented, however, there are also several false positives and false negatives.

Appendix F Supplementary Results

F.1 Baseline CVR maps of all included patients
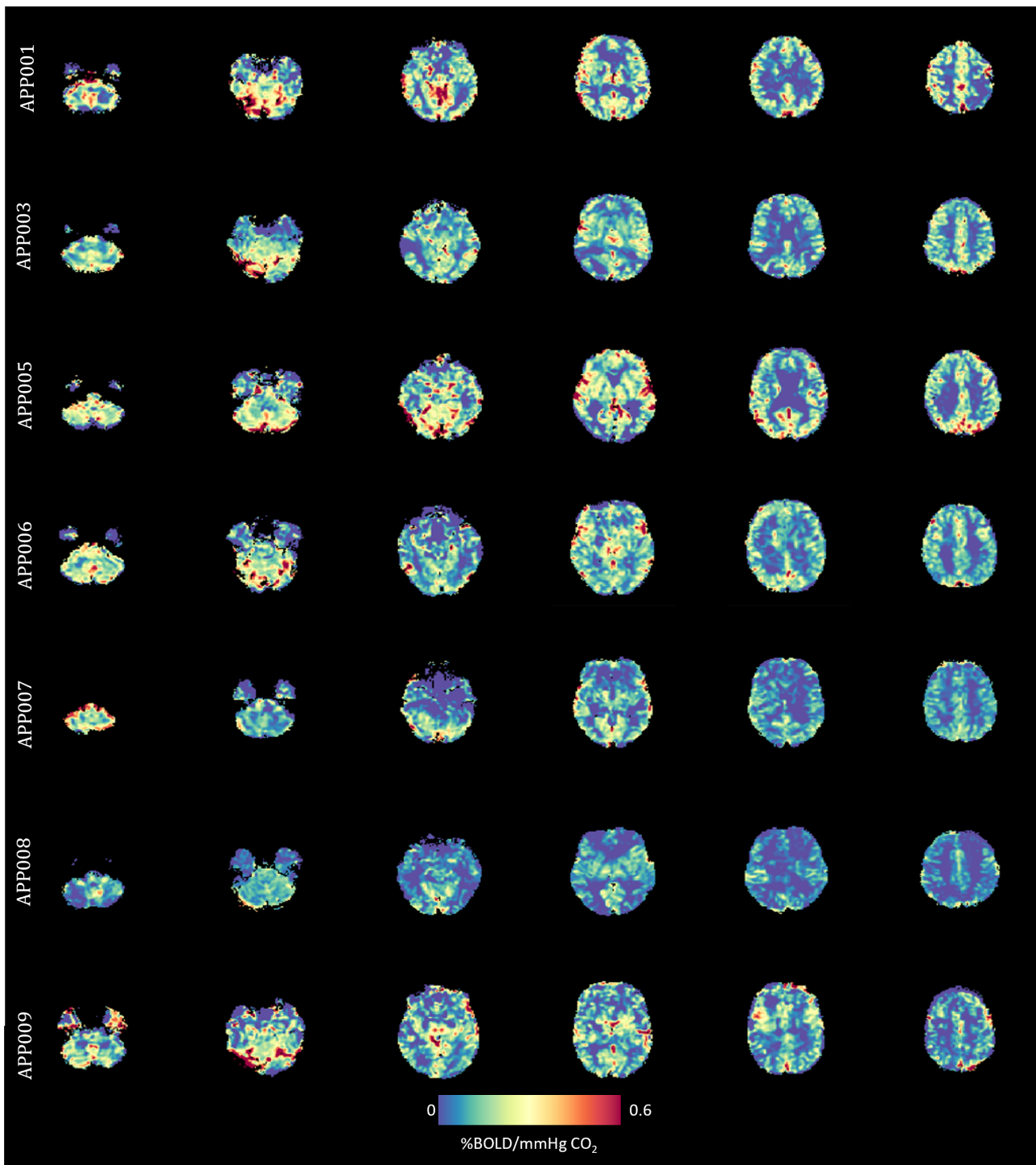
Fig. 30. CVR maps of the baseline patients APP001 to APP009, excluding patients APP002, and APP004.
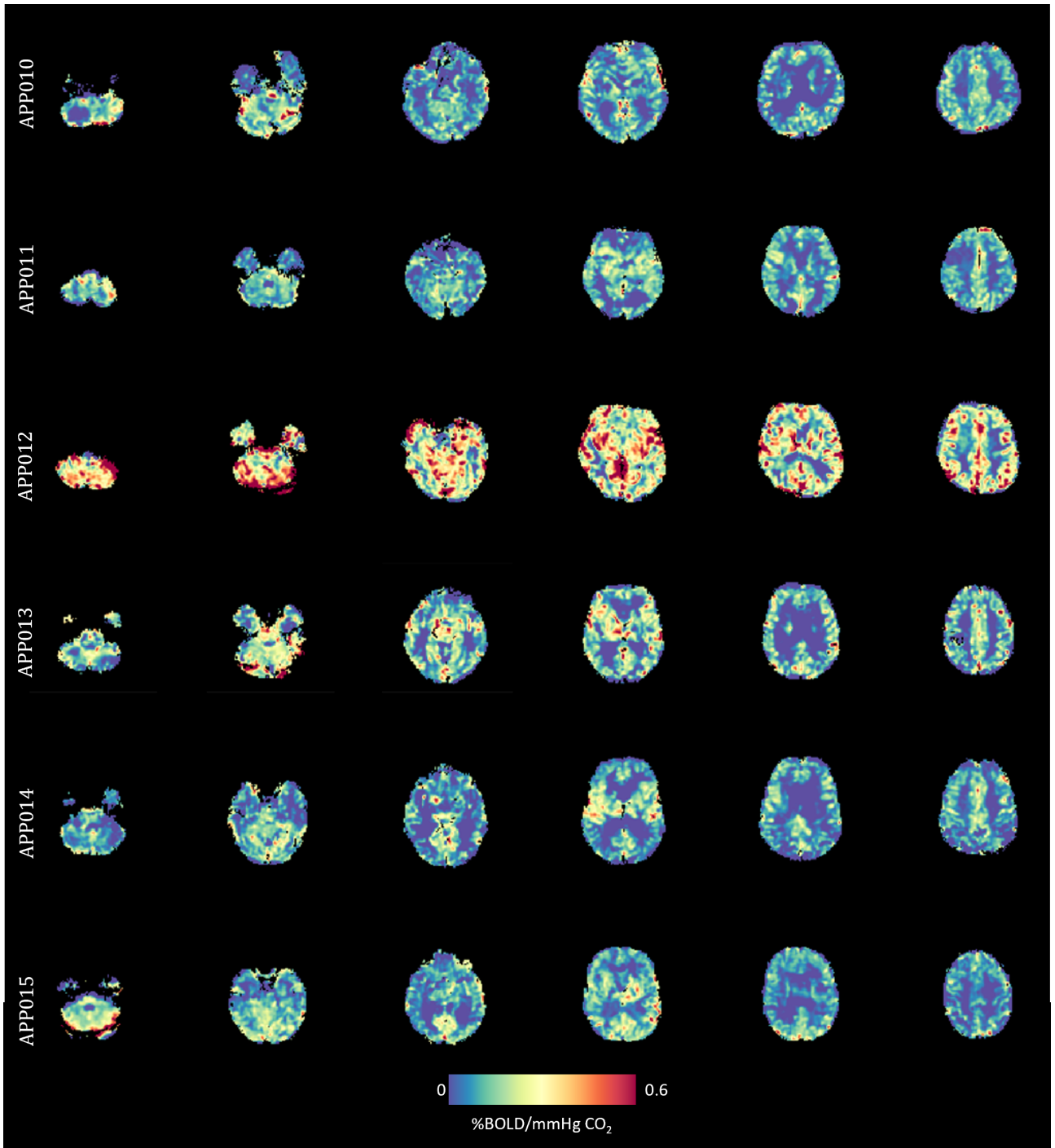
Fig. 31. CVR maps of the baseline patients APP010 to APP015

F.2 Baseline and Follow-up CVR maps of all patients with a follow-up scan

(a)

(b)

(c)
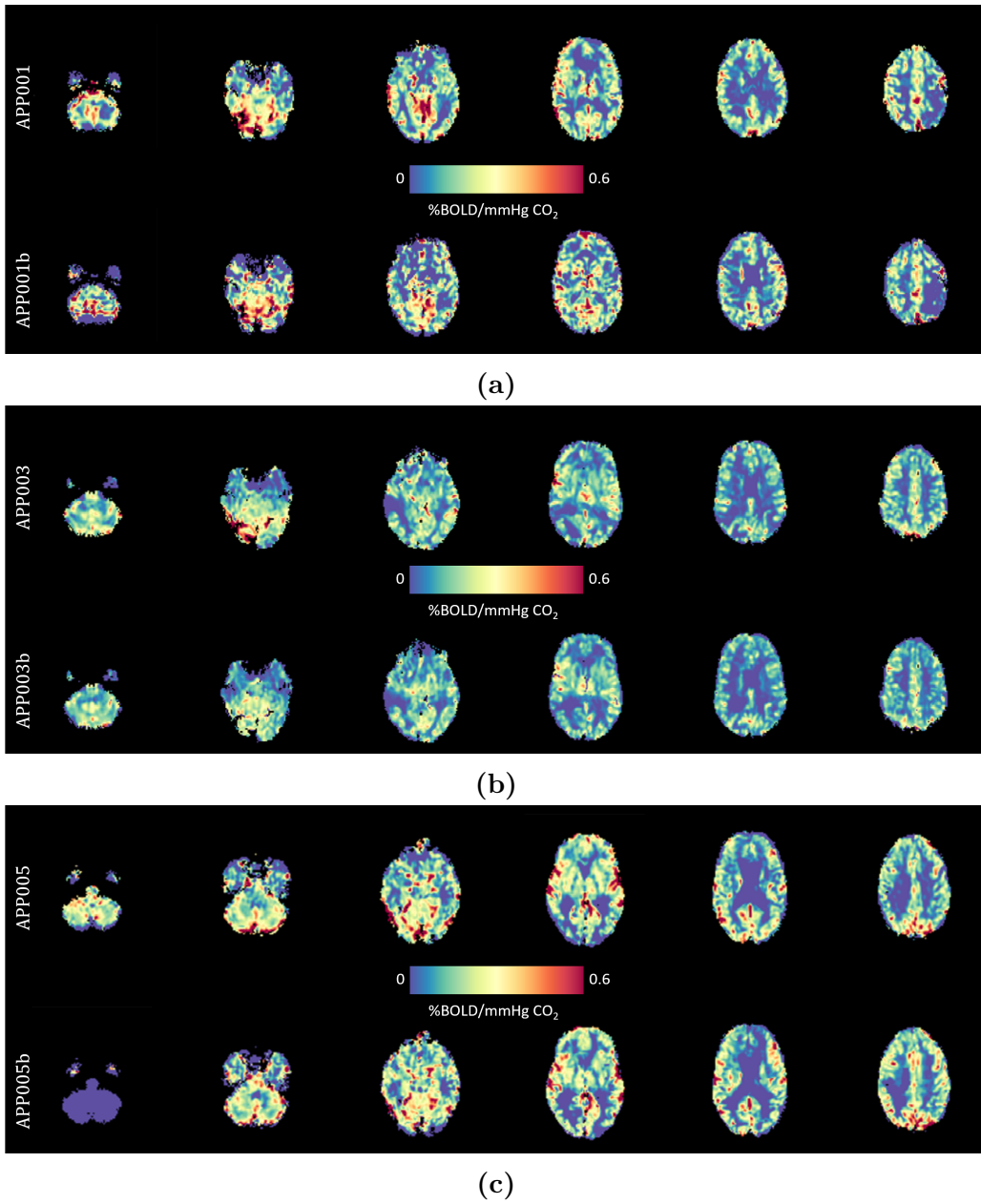
Fig. 32. Baseline and Follow-up CVR maps of APP001, APP003, and APP005
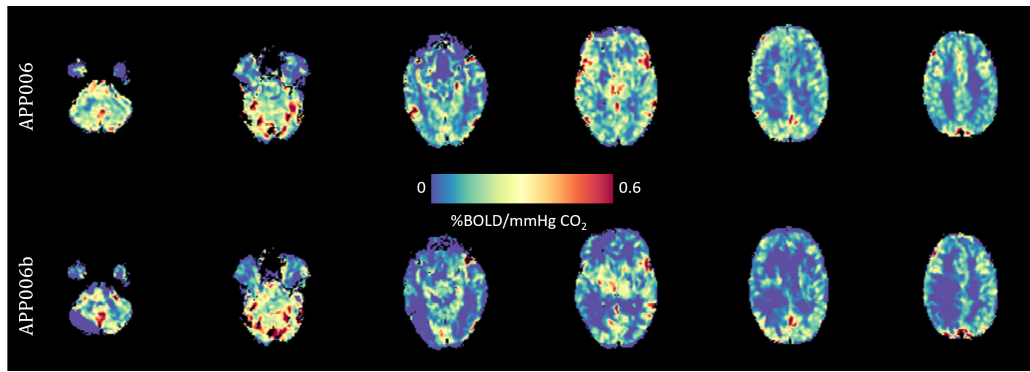
(a)
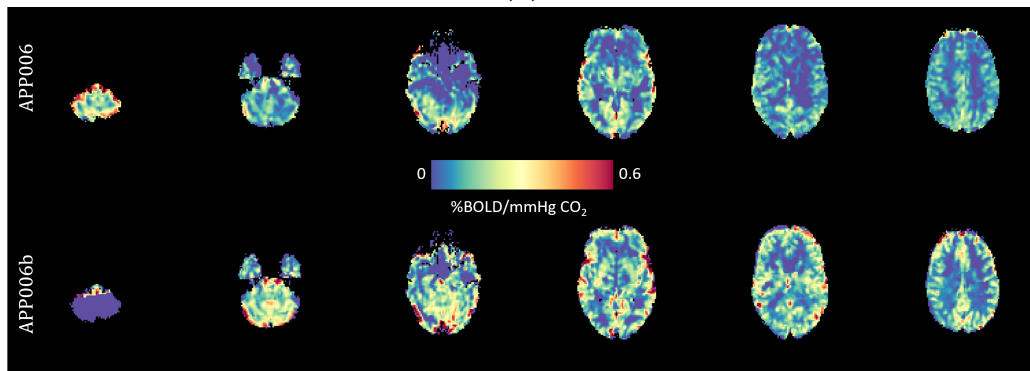
(b)

Fig. 33. Baseline and Follow-up CVR maps of APP006, and APP007

Appendix G   Scripts for Image Registration Pipeline

G.1   Baseline pipeline

Listing 1: Baseline pipeline

```bash
#!/bin/bash
##Pipeline takes 1 hour and 30 min.
##ensure nii files with correct names and location
##T1 folder with T1.nii.gz, T2FLAIR folder with T2FLAIR.nii.gz
##BOLD folder with BOLD.nii.gz and BOLDAPA.nii.gz
##CT folder with CT.nii.gz, dosemap.nii.gz and mask.nii.gz
##input APRICOT patient ID (e.g. bash pipeline.bash APP001)

VDIR=$PWD
cd ${VDIR}/$1

##REGISTRATION CT to T1w
##CT to T1
flirt -in CT/CT -ref T1/T1 -out CT/CTtoT1 -omat CT/CTtoT1.mat -
   cost normmi -v -dof 12 -finesearch 2 -interp trilinear
##Dosemap to T1
flirt -in CT/dosemap -ref T1/T1 -out CT/dosetoT1 -init CT/CTtoT1.
   mat -applyxfm -v -interp nearestneighbour
##Mask to T1
flirt -in CT/mask -ref T1/T1 -out CT/masktoT1 -init CT/CTtoT1.mat
    -applyxfm -v -interp nearestneighbour

##REGISTRATION FLAIR to T1
cd ${VDIR}/$1
##Extract brain FLAIR
bet T2FLAIR/T2FLAIR T2FLAIR/T2FLAIR_brain -R -f 0.4 -g 0 -m
##Extract brain T1
bet T1/T1 T1/T1_brain -R -f 0.4 -g 0 -m
#Create restored bias field for edema segmentation
fast -B -t 2 --nopve T2FLAIR/T2FLAIR.nii.gz
##FLAIR to T1
flirt -in T2FLAIR/T2FLAIR_brain -ref T1/T1_brain -out T2FLAIR/
   T2FLAIRtoT1_brain -omat T2FLAIR/T2FLAIRtoT1_brain.mat -cost
   normcorr -v -dof 6 -interp trilinear
flirt -in T2FLAIR/T2FLAIR -ref T1/T1 -out T2FLAIR/T2FLAIRtoT1 -
   init T2FLAIR/T2FLAIRtoT1_brain.mat -applyxfm -cost normcorr -v
    -dof 6 -interp trilinear

##TOPUP for BOLD
cd ${VDIR}/$1/BOLD
```

```
##Motion correction
mcflirt -in BOLD -out BOLD_mcf -bins 256 -cost leastsquares -dof
    12 -plots -report
##Apply topup to motion corrected timeseries with first volume
fslroi BOLD_mcf B_dn 0 1
fslroi BOLDAPA B_up 0 1
fslmerge -t B_ALL B_dn B_up
##Make parameter file (010 phase encoding direction in y
    direction, minus - or + blip and 0.030 total read out time)
printf "0 -1 0 0.030\n0 1 0 0.030"> acq_params.txt
##Do the topup and apply
topup --imain=B_ALL --datain=acq_params.txt --out=
    my_topup_results --config=b02b0_1.cnf
applytopup --imain=BOLD_mcf --datain=acq_params.txt --inindex=1
    --topup=my_topup_results --method=jac --datatype=float --out=
    BOLD_applytopup
##Create new mean brain image after topup
fslmaths BOLD_applytopup -Tmean BOLD_mean
bet BOLD_mean BOLD_mean_brain -f 0.2 -m
fslmaths BOLD_mcf -Tmean BOLD_pretopup_mean
rm B_ALL.nii.gz B_dn.nii.gz B_up.nii.gz

##REGISTRATION BOLD to T1
cd ${VDIR}/$1
#Create segmentations
fast -t 1 -I 6 -g -B --nopve -o T1/T1 T1/T1_brain
##Registration
epi_reg --epi=BOLD/BOLD_mean --t1=T1/T1 --t1brain=T1/T1_brain --
    out=BOLD/BOLDtoT1_epi --gdc=my_topup_results_fieldcoef --
    echospacing=0.00060 --pedir=-y --noclean --wmseg=T1/T1_seg_2 -
    v
##Remove eyes in BOLD with T1 brain mask
fslmaths T1/T1_brain_mask -mul BOLD/BOLDtoT1_epi BOLD/
    BOLDtoT1_epi_noeyes

##CONVERT T1 segmentations to BOLD space
cd ${VDIR}/$1
#Inverse matrix for epi_reg
convert_xfm -omat BOLD/T1toBOLD.mat -inverse BOLD/BOLDtoT1_epi.
    mat
#Registrations of seg to BOLD space
flirt -in T1/T1_seg_0 -ref BOLD/BOLD_mean_brain -out BOLD/
    seg0toBOLD -init BOLD/T1toBOLD.mat -applyxfm -v -dof 6 -interp
     nearestneighbour
flirt -in T1/T1_seg_1 -ref BOLD/BOLD_mean_brain -out BOLD/
```

```
    seg1toBOLD -init BOLD/T1toBOLD.mat -applyxfm -v -dof 6 -interp
      nearestneighbour
flirt -in T1/T1_seg_2 -ref BOLD/BOLD_mean_brain -out BOLD/
    seg2toBOLD -init BOLD/T1toBOLD.mat -applyxfm -v -dof 6 -interp
      nearestneighbour


##Convert dose and mask (CT) to BOLD space
cd ${VDIR}/$1
##Multiply matrices CTtoT1 and T1toBOLD
convert_xfm -omat CT/CTtoBOLD.mat -concat BOLD/T1toBOLD.mat CT/
    CTtoT1.mat
##Register mask and dose to BOLD space
flirt -in CT/mask -ref BOLD/BOLD_mean_brain -out CT/masktoBOLD -
    init CT/CTtoBOLD.mat -cost normmi -applyxfm -v -dof 6 -interp
      nearestneighbour
flirt -in CT/dosemap -ref BOLD/BOLD_mean_brain -out CT/dosetoBOLD
     -init CT/CTtoBOLD.mat -cost normmi -applyxfm -v -dof 6 -
    interp nearestneighbour
```

G.2 Follow-up pipeline

Listing 2: Follow-up pipeline

```
#!/bin/bash
##PIPELINE FOR FOLLOWUPSCANS
##RUN ONLY AFTER PIPELINE.BASH
##ensure nii files with correct names and location
##T1 folder with T1.nii.gz, T2FLAIR folder with T2FLAIR.nii.gz
##BOLD folder with BOLD.nii.gz and BOLDAPA.nii.gz
##input APRICOT patient ID without b (e.g. bash pipeline_followup
    .bash APP001)


VDIR=$PWD
cd ${VDIR}/$1b


##REGISTRATION T1b (follow-up) to T1
cd ${VDIR}/$1b
##Extract brain
bet T1/T1 T1/T1_brain -R -f 0.4 -g 0 -m
##T1b to T1sub
cd ${VDIR}/
flirt -in $1b/T1/T1_brain -ref $1/T1/T1_brain -out $1b/T1/
    T1btoT1_brain -omat $1b/T1/T1btoT1_brain.mat -v -dof 6 -cost
    normcorr -interp trilinear
```

```
flirt -in $1b/T1/T1 -ref $1/T1/T1 -out $1b/T1/T1btoT1 -init $1b/
   T1/T1btoT1_brain.mat -applyxfm -v -dof 6 -cost normcorr -
   interp trilinear

##TOPUP for BOLDb
cd ${VDIR}/$1b/BOLD
##Motion correction
mcflirt -in BOLD -out BOLD_mcf  -bins 256 -cost leastsquares -dof
    12 -plots -report
##Apply topup to motion corrrected timeseries with first volume
fslroi BOLD_mcf B_dn 0 1
fslroi BOLDAPA B_up 0 1
fslmerge -t B_ALL B_dn B_up
##Make parameter file 010 phase encoding direction , minus - or +
   blip and 0.030 total read out time
printf "0 -1 0 0.030\n0 1 0 0.030"> acq_params.txt
##Do the topup and apply
topup --imain=B_ALL --datain=acq_params.txt --out=
   my_topup_results --config=b02b0_1.cnf
applytopup --imain=BOLD_mcf --datain=acq_params.txt --inindex=1
   --topup=my_topup_results --method=jac --datatype=float --out=
   BOLD_applytopup
##Create new mean brain image after topup
fslmaths BOLD_applytopup -Tmean BOLD_mean
bet BOLD_mean BOLD_mean_brain -f 0.2 -m
rm B_ALL.nii.gz B_dn.nii.gz B_up.nii.gz

##REGISTRATION BOLDb to T1
cd ${VDIR}/$1b
##Step1 register BOLDb to T1b
epi_reg --epi=BOLD/BOLD_mean --t1=T1/T1 --t1brain=T1/T1_brain --
   out=BOLD/BOLDbtoT1b_epi --echospacing=0.00060 --pedir=-y --
   noclean --wmseg=T1/T1_seg_2 -v
##Step2 combine matrix T1b to T1 and BOLDb to T1b
convert_xfm -omat BOLD/BOLDbtoT1_basline.mat -concat T1/
   T1btoT1_brain.mat BOLD/BOLDbtoT1b_epi.mat
##Step3 regiser BOLDb to T1
cd ${VDIR}/
flirt -in $1b/BOLD/BOLD_mean -ref $1/T1/T1_brain -init $1b/BOLD/
   BOLDbtoT1_basline.mat -out $1b/BOLD/BOLDbtoT1 -applyxfm -v -
   dof 6 -cost normmi -finesearch 5 -echospacing 0.00060 -pedir
   -2 -interp spline
##Remove eyes in BOLD with T1 brain mask
fslmaths $1/T1/T1_brain_mask -mul $1b/BOLD/BOLDbtoT1 $1b/BOLD/
   BOLDbtoT1_noeyes
```

```
##REGISTRATION T2FLAIRb to T1
cd ${VDIR}/$1b
##Extract brain T2FLAIR
bet T2FLAIR/T2FLAIR T2FLAIR/T2FLAIR_brain -R -f 0.4 -g 0 -m
##T2FLAIRb to T1
cd ${VDIR}/
flirt -in $1b/T2FLAIR/T2FLAIR_brain -ref $1/T1/T1_brain -out $1b/
    T2FLAIR/T2FLAIRbtoT1_brain -omat $1b/T2FLAIR/
    T2FLAIRbtoT1_brain.mat -v -cost normmi -dof 6 -interp
    trilinear
flirt -in $1b/T2FLAIR/T2FLAIR -ref $1/T1/T1 -out $1b/T2FLAIR/
    T2FLAIRbtoT1 -init $1b/T2FLAIR/T2FLAIRbtoT1_brain.mat -
    applyxfm -v -dof 6 -interp trilinear

##FOR SEGMENTATIONS SeeVR
cd ${VDIR}/$1b
##Extract seggmentations brain T1b
fast -t 1 -I 6 -g --nopve -o T1/T1 T1/T1_brain
##CONVERT T1b segmentations to BOLDb space
cd ${VDIR}/$1b
##Inverse matrix for epi_reg
convert_xfm -omat BOLD/T1btoBOLDb.mat -inverse BOLD/
    BOLDbtoT1b_epi.mat
##Registrations of seg to BOLD space
flirt -in T1/T1_seg_0 -ref BOLD/BOLD_mean -out BOLD/seg0toBOLD -
    init BOLD/T1btoBOLDb.mat -applyxfm -v -interp nearestneighbour
flirt -in T1/T1_seg_1 -ref BOLD/BOLD_mean -out BOLD/seg1toBOLD -
    init BOLD/T1btoBOLDb.mat -applyxfm -v -interp nearestneighbour
flirt -in T1/T1_seg_2 -ref BOLD/BOLD_mean -out BOLD/seg2toBOLD -
    init BOLD/T1btoBOLDb.mat -applyxfm -v -interp nearestneighbour
```

Appendix H   Scripts and Functions for Data Analysis

H.1   Data Analysis

<div align="center">Listing 3: Data Analysis Script</div>

```matlab
close all; clear all;

numPT = 15; %number of total patients
numPTfollow=7; %number of patients that have a follow-up

%Create PT list for baseline
PTnumbers=strcat('APP', cellfun(@(x) sprintf('%03d',x),num2cell(1:numPT),
    'UniformOutput',false)); %make APP list

%Remove PT with insufficient data
PTnumbers(2)=[]; %Artefacts in CVR APP002
PTnumbers(3)=[]; %no BOLD data APP004

%Create PT list for follow-up
PTnumbersfollow=strcat('APP', cellfun(@(x) sprintf('%03d',x),num2cell(1:
    numPTfollow),'UniformOutput',false)); %make APP list

%Remove PT with insufficient data
PTnumbersfollow(2)=[]; %Artefacts in baseline therefore cannot compare
    these two
PTnumbersfollow(3)=[]; %No follow-up, PT could not do the BOLD scan..

%%

%BASELINE ANALYSIS OF SEGMENTATIONS AROUND TUMOUR MASK (BOLD SPACE)
%Create segmentations around the tumour (increasing with 2 pixels)

for m=1:numel(PTnumbers)
    vnumber = char(PTnumbers(m))
    [var, voigm, voiwm, voi_noed] = stepstumourmask_bold(vnumber);
    [meanCVRgmvoi(m,:), meanCVRwmvoi(m,:), meanCVRallvoi(m,:),
        meanCVR_noedvoi(m,:)] = meanCVRtumourseg_bold(var, voigm, voiwm,
        voi_noed, vnumber);
end

%Create new dir to save results
dir.anl = ['/Fridge/users/alex/APRICOT/jamila_analysis/'];

dir.voimeancvr = [dir.anl, 'voimeanCVR/'];
if ~exist(dir.voimeancvr,'dir')
    mkdir(dir.voimeancvr)
end
```

```matlab
38
39  %Save results in new dir
40  writematrix(meanCVRallvoi,[dir.voimeancvr,'meanCVRallvoi.csv']); save([
        dir.voimeancvr,'meanCVRallvoi.mat'])
41  writematrix(meanCVRgmvoi,[dir.voimeancvr,'meanCVRgmvoi.csv']); save([dir.
        voimeancvr,'meanCVRgmvoi.mat'])
42  writematrix(meanCVRwmvoi,[dir.voimeancvr,'meanCVRwmvoi.csv']); save([dir.
        voimeancvr,'meanCVRwmvoi.mat'])
43  writematrix(meanCVR_noedvoi,[dir.voimeancvr,'meanCVR_noedvoi.csv']); save
        ([dir.voimeancvr,'meanCVR_noedvoi.mat'])
44
45  %%
46
47  % % COMPARISON FOLLOW_UP AND BASELINE dose segmentations (BASELINE BOLD
        SPACE)
48  % %This for loop creates dose segmentaions and the average CVR value per
        voi per patient
49  for j=1:numel(PTnumbersfollow)
50      vnumber = char(PTnumbersfollow(j))
51      [thresdoseall, thresdosegm, thresdosewm, thresdose_noed, tot_gm(j,:),
            tot_wm(j,:), tot_noed(j,:)] = voidoseCVR(vnumber);
52      [meanCVRgmdose(j,:), meanCVRwmdose(j,:), meanCVRalldose(j,:),
            meanCVRgmdoseb(j,:), meanCVRwmdoseb(j,:), meanCVRalldoseb(j,:),
            meanCVRnoeddose(j,:), meanCVRnoeddoseb(j,:)] = voidoseCVRcal(
            thresdoseall, thresdosegm, thresdosewm, thresdose_noed, vnumber);
53  end
54
55  %save results in new dir
56  dir.anl = ['/Fridge/users/alex/APRICOT/jamila_analysis/'];
57
58  dir.dosevoimeancvr = [dir.anl, 'dosevoimeanCVR/'];
59  if ~exist(dir.dosevoimeancvr,'dir')
60      mkdir(dir.dosevoimeancvr)
61  end
62
63  %Save baseline data
64  writematrix(meanCVRgmdose,[dir.dosevoimeancvr,'meanCVRgmdose.csv']); save
        ([dir.dosevoimeancvr,'meanCVRgmdose.mat'])
65  writematrix(meanCVRwmdose,[dir.dosevoimeancvr,'meanCVRwmdose.csv']); save
        ([dir.dosevoimeancvr,'meanCVRwmdose.mat'])
66  writematrix(meanCVRalldose,[dir.dosevoimeancvr,'meanCVRalldose.csv']);
        save([dir.dosevoimeancvr,'meanCVRalldose.mat'])
67  writematrix(meanCVRalldose,[dir.dosevoimeancvr,'meanCVRnoeddose.csv']);
        save([dir.dosevoimeancvr,'meanCVRnoeddose.mat'])
68
69  %Save followup data
70  writematrix(meanCVRgmdoseb,[dir.dosevoimeancvr,'meanCVRgmdoseb.csv']);
        save([dir.dosevoimeancvr,'meanCVRgmdoseb.mat'])
```

```matlab
71  writematrix(meanCVRwmdoseb,[dir.dosevoimeancvr,'meanCVRwmdoseb.csv']);
        save([dir.dosevoimeancvr,'meanCVRwmdoseb.mat'])
72  writematrix(meanCVRalldoseb,[dir.dosevoimeancvr,'meanCVRalldoseb.csv']);
        save([dir.dosevoimeancvr,'meanCVRalldoseb.mat'])
73  writematrix(meanCVRalldoseb,[dir.dosevoimeancvr,'meanCVRnoeddoseb.csv']);
        save([dir.dosevoimeancvr,'meanCVRnoeddoseb.mat'])
74
75  %Save number of voxels in dose groups
76  writematrix(tot_gm,[dir.dosevoimeancvr,'tot_gm.csv']); save([dir.
        dosevoimeancvr,'tot_gm.mat'])
77  writematrix(tot_wm,[dir.dosevoimeancvr,'tot_wm.csv']); save([dir.
        dosevoimeancvr,'tot_wm.mat'])
78  writematrix(tot_noed,[dir.dosevoimeancvr,'tot_noed.csv']); save([dir.
        dosevoimeancvr,'tot_noed.mat'])
```

H.2 Creation of Volume of Interests

Listing 4: Create VOIs around Tumour

```matlab
1  function [var2, voigm, voiwm, voi_noed] = stepstumourmask_bold(vnumber)
2  %This script creates segmentations or 2 pixels around the tumour (max is
       14 pixels away from GTV)
3
4  %Load data
5
6  %Load CT data
7  dir.ct = ['/Fridge/users/alex/APRICOT/',vnumber,'/CT/'];
8  [mask, info.mask, header.mask] = loadImageData(dir.ct, 'masktoBOLD.nii.gz
       '); %Load mask of tumours
9
10  %Load CVR brainmask
11  dir.cvr = ['/Fridge/users/alex/APRICOT/',vnumber,'/BOLD/
       CO2BLOCK_GS0_WD1_CO2pr1/'];
12  [brainmask, info.brainmask, header.brainmask] = loadImageData(dir.cvr,'
       mWBmask*.nii.gz');
13
14  %Load CSF and WM information
15  dir.bold = ['/Fridge/users/alex/APRICOT/',vnumber,'/BOLD/'];
16  [wm, info.wm, header.wm] = loadImageData(dir.bold,'seg2toBOLD.nii.gz');
17  [csf, info.csf, header.csf] = loadImageData(dir.bold,'seg0toBOLD.nii.gz')
       ;
18
19  %Load T1 dir
20  dir.t1 = ['/Fridge/users/alex/APRICOT/',vnumber,'/T1/'];
21
22  if isfile([dir.t1,'gmtoBOLD.nii.gz'])
23      [seggm, info.seggm, header.seggm] = loadImageData(dir.t1, 'gmtoBOLD.
           nii.gz');
```

```matlab
24    [ed, info.ed, header.ed] = loadImageData(dir.t1, 'edtoBOLD.nii.gz');
          %Load edema in BOLD space
25  else
26      %Load edema and GM information in T1 space
27      [edema, info.edema, header.edema] = loadImageData(dir.t1,'
          edema_semiauto.nii.gz');
28      [gm, info.gm, header.gm] = loadImageData(dir.t1,'T1_seg_1.nii.gz');
29      %Load tumour mask in T1 space
30      [maskt1, info.maskt1, header.maskt1] = loadImageData(dir.ct, '
          masktoT1.nii.gz');

31
32      newgm= gm.*not(edema).*not(maskt1);
33      saveImageData(newgm, header.gm, dir.t1, 'newgm.nii.gz', 64)

34
35      %Register the newgm in BOLD space and reload
36      cmd = ['bash', ' ','newgmtoBOLD.bash', ' ' , vnumber];   %you can
          check the segmentation in T1 directory
37      system (cmd);
38      [seggm, info.seggm, header.seggm] = loadImageData(dir.t1, 'gmtoBOLD.
          nii.gz'); %Load new GM (no edema, no tumour) in BOLD space
39      [ed, info.ed, header.ed] = loadImageData(dir.t1, 'edtoBOLD.nii.gz');
          %Load edema in BOLD space
40  end

41
42  %%

43
44  %Create segmentations around the tumor mask
45  A=[2 4 6 8 10 12 14]; %increasing steps of 2 pixels
46  evmask=mask; %create newmask
47  evmask(mask>1)=0; %only using GTV not PTV
48  var=struct('voi1',{0},'voi2',{0},'voi3',{0},'voi4',{0},'voi5',{0});
49  var2=struct('voi1',{0},'voi2',{0},'voi3',{0},'voi4',{0},'voi5',{0});

50
51  for i=1:length(A)
52      SE(i)=strel('sphere',A(i));
53      voi=sprintf('voi%d',i);  voimin=sprintf('voi%d',i-1);
54      var.(voi)=imdilate(evmask,SE(i));
55      if i==1
56          var2.(voi)=var.(voi)-evmask;
57      else
58          var2.(voi)=((var.(voi)-var.(voimin)));
59      end
60  end

61
62  voigm = var2;
63  voiwm = var2;
64  voi_noed = var2;

65
```

```
66  for i=1:length(A)
67      voi = sprintf('voi%d',i);
68      %Create GM and WM the masks
69      voigm.(voi)(seggm==0)=0; voiwm.(voi)(wm==0)=0;
70      %Exclude pixels outside the brain
71      var2.(voi)(brainmask==0)=0; voigm.(voi)(brainmask==0)=0; voiwm.(voi)(
            brainmask==0)=0; voi_noed.(voi)(brainmask==0)=0;
72      %Exclude pixels inside CSF
73      var2.(voi)(csf==1)=0; voiwm.(voi)(csf==1)=0; voigm.(voi)(csf==1)=0;
            voi_noed.(voi)(csf==1)=0;
74      %exclude Edema for 'All' mask
75      voi_noed.(voi)(ed==1)=0;
76  end
77
78  %Check segmentations to see if they are correct
79  %Save in CT dir
80  segmentations_all=var2.voi1+var2.voi2.*2+var2.voi3.*3+var2.voi4.*4+var2.
        voi5.*5+var2.voi6.*6+var2.voi7.*7;
81  saveImageData(segmentations_all, header.mask, dir.ct, 'segmentations_all.
        nii.gz', 64)
82  segmentations_gm=voigm.voi1+voigm.voi2.*2+voigm.voi3.*3+voigm.voi4.*4+
        voigm.voi5.*5+voigm.voi6.*6+voigm.voi7.*7;
83  saveImageData(segmentations_gm, header.mask, dir.ct, 'segmentations_gm.
        nii.gz', 64)
84  segmentations_wm=voiwm.voi1+voiwm.voi2.*2+voiwm.voi3.*3+voiwm.voi4.*4+
        voiwm.voi5.*5+voiwm.voi6.*6+voiwm.voi7.*7;
85  saveImageData(segmentations_wm, header.mask, dir.ct, 'segmentations_wm.
        nii.gz', 64)
86  segmentations_noed=voi_noed.voi1+voi_noed.voi2.*2+voi_noed.voi3.*3+
        voi_noed.voi4.*4+voi_noed.voi5.*5+voi_noed.voi6.*6+voi_noed.voi7.*7;
87  saveImageData(segmentations_noed, header.mask, dir.ct, '
        segmentations_noed.nii.gz', 64)
88
89  end
```

H.3   Calculation VOI-Based Analysis

Listing 5: Calculate Mean CVR in VOIs

```
1  function [meanCVRgmvoi, meanCVRwmvoi, meanCVRallvoi, meanCVR_noedvoi] =
       meanCVRtumourseg_bold(var, voigm, voiwm, voi_noed, vnumber)
2  %This script calculates the mean CVR in each VOI around the tumour
3
4  %Load baseline data
5
6  %Load registered BOLD data
7  %Load CVR data
```

```matlab
8   dir.cvr = ['/Fridge/users/alex/APRICOT/',vnumber,'/BOLD/
        CO2BLOCK_GS0_WD1_CO2pr1/corrLAG/CVR/'];
9   [CVR, info.cvr, header.cvr] = loadImageData(dir.cvr, 'bCVR_map.nii.gz');
10
11  dir.bm = ['/Fridge/users/alex/APRICOT/',vnumber,'/BOLD/
        CO2BLOCK_GS0_WD1_CO2pr1/'];
12  [brainmask, info.brainmask, header.brainmask] = loadImageData(dir.bm, '
        mWBmask*.nii.gz');
13
14  %%
15
16  CVR(brainmask == 0) = nan;
17
18  %%
19  %Calculate mean CVR value per segmentation
20  for i = 1:length(fieldnames(var))
21      voi=sprintf('voi%d',i);
22
23      cvrgm.(voi) = voigm.(voi).*CVR; cvrgm.(voi)(voigm.(voi) == 0) = nan;
24      cvrgm.(voi) = cvrgm.(voi)(~isnan(cvrgm.(voi)));
25      meanCVRgmvoi(i) = mean(cvrgm.(voi));
26
27      cvrwm.(voi) = voiwm.(voi).*CVR; cvrwm.(voi)(voiwm.(voi) == 0) = nan;
28      cvrwm.(voi) = cvrwm.(voi)(~isnan(cvrwm.(voi)));
29      meanCVRwmvoi(i) = mean(cvrwm.(voi));
30
31      cvr_noed.(voi) = voi_noed.(voi).*CVR; cvr_noed.(voi)(voi_noed.(voi)
          == 0) = nan;
32      cvr_noed.(voi) = cvr_noed.(voi)(~isnan(cvr_noed.(voi)));
33      meanCVR_noedvoi(i) = mean(cvr_noed.(voi));
34
35      cvrall.(voi) = var.(voi).*CVR; cvrall.(voi)(var.(voi) == 0) = nan;
36      cvrall.(voi) = cvrall.(voi)(~isnan(cvrall.(voi)));
37      meanCVRallvoi(i) = mean(cvrall.(voi));
38  end
39
40  %save results in new dir
41  dir.bold = ['/Fridge/users/alex/APRICOT/',vnumber,'/BOLD/'];
42  dir.calcu = [dir.bold, 'CVRcalculations/'];
43  if ~exist(dir.calcu,'dir')
44      mkdir(dir.calcu)
45  end
46
47  save([dir.calcu,'meanCVRallvoi.mat'])
48  save([dir.calcu,'meanCVRgmvoi.mat'])
49  save([dir.calcu,'meanCVRwmvoi.mat'])
50  save([dir.calcu,'meanCVR_noedvoi.mat'])
51  end
```

H.4 Creation of Dose Regions

Listing 6: Creation of Dose Regions

```matlab
function [thresdoseall, thresdosegm, thresdosewm, thresdose_noed] =
    voidoseCVR(vnumber)
%This script creates segmentations of the dose
%The dose groups were selected after a discussion with the research team
%(including a radiation oncologist and medical physicist)

%Load CT data
dir.ct = ['/Fridge/users/alex/APRICOT/',vnumber,'/CT/'];
[mask, info.mask, header.mask] = loadImageData(dir.ct, 'masktoBOLD.nii.gz
    ');
[dose, info.dose, header.dose] = loadImageData(dir.ct, 'dosetoBOLD.nii.gz
    ');

%Load CVR brainmask
dir.cvr = ['/Fridge/users/alex/APRICOT/',vnumber,'/BOLD/
    CO2BLOCK_GS0_WD1_CO2pr1/'];
[brainmask, info.brainmask, header.brainmask] = loadImageData(dir.cvr,'
    mWBmask*.nii.gz');

%Load CSF and WM information
dir.bold = ['/Fridge/users/alex/APRICOT/',vnumber,'/BOLD/'];
[wm, info.wm, header.wm] = loadImageData(dir.bold,'seg2toBOLD.nii.gz');
[csf, info.csf, header.csf] = loadImageData(dir.bold,'seg0toBOLD.nii.gz')
    ;

%Load T1 dir
dir.t1 = ['/Fridge/users/alex/APRICOT/',vnumber,'/T1/'];

if isfile([dir.t1,'gmtoBOLD.nii.gz'])
    [seggm, info.seggm, header.seggm] = loadImageData(dir.t1, 'gmtoBOLD.
        nii.gz');
    [ed, info.ed, header.ed] = loadImageData(dir.t1, 'edtoBOLD.nii.gz');
        %Load edema in BOLD space
else
    %Load edema and GM information in T1 space
    [edema, info.edema, header.edema] = loadImageData(dir.t1,'
        edema_semiauto.nii.gz');
    [gm, info.gm, header.gm] = loadImageData(dir.t1,'T1_seg_1.nii.gz');
    %Load tumour mask in T1 space
    [maskt1, info.maskt1, header.maskt1] = loadImageData(dir.ct, '
        masktoT1.nii.gz');

    newgm= gm.*not(edema).*not(maskt1);
    saveImageData(newgm, header.gm, dir.t1, 'newgm.nii.gz', 64)
```

69

```matlab
35
36        %Register the newgm in BOLD space and reload
37        cmd = ['bash', ' ','newgmtoBOLD.bash', ' ' , vnumber];  %you can
              check the segmentation in T1 directory
38        system (cmd);
39        [seggm, info.seggm, header.seggm] = loadImageData(dir.t1, 'gmtoBOLD.
              nii.gz'); %Load new GM (no edema, no tumour) in BOLD space
40        [ed, info.ed, header.ed] = loadImageData(dir.t1, 'edtoBOLD.nii.gz');
              %Load edema in BOLD space
41  end
42
43
44  %%
45  %Create dose segmentations for GM, WM and all
46  %Values to detemine the dose segmentation groups
47  idx = [5 8 12 16];
48
49  %Create vois based on idx values
50  thresdose = struct('voi1', {dose<idx(1)}, 'voi2', {dose>=idx(1) & dose<
        idx(2)}, 'voi3', {dose>=idx(2) & dose<idx(3)}, 'voi4',{dose>=idx(3) &
        dose<idx(4)}, 'voi5', {dose>=idx(4)});
51
52  %Create masks of dose based on the GM, WM, CSF and brainmask
53  for i = 1:length(idx)+1
54        voi=sprintf('voi%d',i);
55        thresdosegm.(voi) = ((thresdose.(voi).*brainmask).*(not(csf)).*seggm
              .*(not(mask)));
56        thresdosewm.(voi) = (thresdose.(voi).*brainmask).*(not(csf)).*wm.*(
              not(mask));
57        thresdose_noed.(voi) = (thresdose.(voi).*brainmask).*(not(csf)).*(not
              (ed));
58        thresdoseall.(voi) = (thresdose.(voi).*brainmask).*(not(csf));
59  end
60
61  voidose_gm = thresdosegm.voi1 + thresdosegm.voi2.*2 + thresdosegm.voi3.*3
        + thresdosegm.voi4.*4 + thresdosegm.voi5.*5;
62  voidose_wm = thresdosewm.voi1 + thresdosewm.voi2.*2 + thresdosewm.voi3.*3
        + thresdosewm.voi4.*4 + thresdosewm.voi5.*5;
63  voidose_noed = thresdose_noed.voi1 + thresdose_noed.voi2.*2 +
        thresdose_noed.voi3.*3 + thresdose_noed.voi4.*4 + thresdose_noed.voi5
        .*5;
64  voidose = thresdoseall.voi1 + thresdoseall.voi2.*2 + thresdoseall.voi3.*3
        + thresdoseall.voi4.*4 + thresdoseall.voi5.*5;
65
66  %Saving the dose segmentations in the CT directory
67  saveImageData(voidose, header.dose, dir.ct, 'voidose.nii.gz', 64)
68  saveImageData(voidose_gm, header.dose, dir.ct, 'voidose_gm.nii.gz', 64)
69  saveImageData(voidose_noed, header.dose, dir.ct, 'voidose_noed.nii.gz',
```

```
        64)
70  saveImageData(voidose_wm, header.dose, dir.ct, 'voidose_wm.nii.gz', 64)
71
72  end
```

H.5 Calculation Dose-Based Analysis

Listing 7: Calculation Mean CVR in Dose regions

```
1  function [thresdoseall, thresdosegm, thresdosewm, thresdose_noed, tot_gm,
        tot_wm, tot_noed] = voidoseCVR(vnumber)
2  %This script creates segmentations of the dose
3  %The dose groups were selected after a discussion with the research team
4  %(including a radiation oncologist and medical physicist)
5
6  %Load CT data
7  dir.ct = ['/Fridge/users/alex/APRICOT/',vnumber,'/CT/'];
8  [mask, info.mask, header.mask] = loadImageData(dir.ct, 'masktoBOLD.nii.gz
        ');
9  [dose, info.dose, header.dose] = loadImageData(dir.ct, 'dosetoBOLD.nii.gz
        ');
10
11  %Load CVR brainmask
12  dir.cvr = ['/Fridge/users/alex/APRICOT/',vnumber,'/BOLD/
        CO2BLOCK_GS0_WD1_CO2pr1/'];
13  [brainmask, info.brainmask, header.brainmask] = loadImageData(dir.cvr,'
        mWBmask*.nii.gz');
14
15  %Load CSF and WM information
16  dir.bold = ['/Fridge/users/alex/APRICOT/',vnumber,'/BOLD/'];
17  [wm, info.wm, header.wm] = loadImageData(dir.bold,'seg2toBOLD.nii.gz');
18  [csf, info.csf, header.csf] = loadImageData(dir.bold,'seg0toBOLD.nii.gz')
        ;
19
20  %Load T1 dir
21  dir.t1 = ['/Fridge/users/alex/APRICOT/',vnumber,'/T1/'];
22
23  if isfile([dir.t1,'gmtoBOLD.nii.gz'])
24      [seggm, info.seggm, header.seggm] = loadImageData(dir.t1, 'gmtoBOLD.
            nii.gz');
25      [ed, info.ed, header.ed] = loadImageData(dir.t1, 'edtoBOLD.nii.gz');
            %Load edema in BOLD space
26  else
27      %Load edema and GM information in T1 space
28      [edema, info.edema, header.edema] = loadImageData(dir.t1,'
            edema_semiauto.nii.gz');
29      [gm, info.gm, header.gm] = loadImageData(dir.t1,'T1_seg_1.nii.gz');
```

```matlab
30      %Load tumour mask in T1 space
31      [maskt1, info.maskt1, header.maskt1] = loadImageData(dir.ct, '
            masktoT1.nii.gz');

32
33      newgm= gm.*not(edema).*not(maskt1);
34      saveImageData(newgm, header.gm, dir.t1, 'newgm.nii.gz', 64)

35
36      %Register the newgm in BOLD space and reload
37      cmd = ['bash', ' ' ,'newgmtoBOLD.bash', ' ' , vnumber];  %you can
            check the segmentation in T1 directory
38      system (cmd);
39      [seggm, info.seggm, header.seggm] = loadImageData(dir.t1, 'gmtoBOLD.
            nii.gz'); %Load new GM (no edema, no tumour) in BOLD space
40      [ed, info.ed, header.ed] = loadImageData(dir.t1, 'edtoBOLD.nii.gz');
            %Load edema in BOLD space
41  end

42
43
44  %%
45  %Create dose segmentations for GM, WM and all
46  %Values to detemine the dose segmentation groups
47  idx = [5 8 12 16];

48
49  %Create vois based on idx values
50  thresdose = struct('voi1', {dose<idx(1)}, 'voi2', {dose>=idx(1) & dose<
        idx(2)}, 'voi3', {dose>=idx(2) & dose<idx(3)}, 'voi4',{dose>=idx(3) &
        dose<idx(4)}, 'voi5', {dose>=idx(4)});

51
52  %Create masks of dose based on the GM, WM, CSF and brainmask
53  for i = 1:length(idx)+1
54      voi=sprintf('voi%d',i);
55      thresdosegm.(voi) = ((thresdose.(voi).*brainmask).*(not(csf)).*seggm
            .*(not(mask)));
56      thresdosewm.(voi) = (thresdose.(voi).*brainmask).*(not(csf)).*wm.*(
            not(mask));
57      thresdose_noed.(voi) = (thresdose.(voi).*brainmask).*(not(csf)).*(not
            (ed));
58      thresdoseall.(voi) = (thresdose.(voi).*brainmask).*(not(csf));
59  end

60
61
62  %% Count number of Voxels in the Dose groups

63
64  tot_gm=ones(1,length(idx)+1);
65  tot_gm(1)=sum(thresdosegm.voi1(:) == 1);
66  tot_gm(2)=sum(thresdosegm.voi2(:) == 1);
67  tot_gm(3)=sum(thresdosegm.voi3(:) == 1);
68  tot_gm(4)=sum(thresdosegm.voi4(:) == 1);
```

```matlab
69  tot_gm(5)=sum(thresdosegm.voi5(:) == 1);

70

71  tot_wm=ones(1,length(idx)+1);
72  tot_wm(1)=sum(thresdosewm.voi1(:) == 1);
73  tot_wm(2)=sum(thresdosewm.voi2(:) == 1);
74  tot_wm(3)=sum(thresdosewm.voi3(:) == 1);
75  tot_wm(4)=sum(thresdosewm.voi4(:) == 1);
76  tot_wm(5)=sum(thresdosewm.voi5(:) == 1);

77

78  tot_noed=ones(1,length(idx)+1);
79  tot_noed(1)=sum(thresdose_noed.voi1(:) == 1);
80  tot_noed(2)=sum(thresdose_noed.voi2(:) == 1);
81  tot_noed(3)=sum(thresdose_noed.voi3(:) == 1);
82  tot_noed(4)=sum(thresdose_noed.voi4(:) == 1);
83  tot_noed(5)=sum(thresdose_noed.voi5(:) == 1);

84

85  %%

86

87  voidose_gm = thresdosegm.voi1 + thresdosegm.voi2.*2 + thresdosegm.voi3.*3
        + thresdosegm.voi4.*4 + thresdosegm.voi5.*5;
88  voidose_wm = thresdosewm.voi1 + thresdosewm.voi2.*2 + thresdosewm.voi3.*3
        + thresdosewm.voi4.*4 + thresdosewm.voi5.*5;
89  voidose_noed = thresdose_noed.voi1 + thresdose_noed.voi2.*2 +
        thresdose_noed.voi3.*3 + thresdosewm.voi4.*4 + thresdose_noed.voi5.*5;
90  voidose = thresdoseall.voi1 + thresdoseall.voi2.*2 + thresdoseall.voi3.*3
        + thresdoseall.voi4.*4 + thresdoseall.voi5.*5;

91

92  %Saving the dose segmentations in the CT directory
93  saveImageData(voidose, header.dose, dir.ct, 'voidose.nii.gz', 64)
94  saveImageData(voidose_gm, header.dose, dir.ct, 'voidose_gm.nii.gz', 64)
95  saveImageData(voidose_noed, header.dose, dir.ct, 'voidose_noed.nii.gz',
        64)
96  saveImageData(voidose_wm, header.dose, dir.ct, 'voidose_wm.nii.gz', 64)

97

98  end
```